University of Cape Town
Faculty of Science
Departments of Oceanography
Thesis presented for the degree of Master of Science

Marine heatwaves and Warm Events in the Cape Peninsula Upwelling Cell, Southern Benguela

Kirstin Robyn Petzer
Student number: PTZKIR001

Supervisors: Dr. Tarron Lamont and Prof. Mathieu Rouault.†

Plagiarism Delegation

I acknowledge the meaning of plagiarism and declare that all the work in this dissertation is my own except for the work of others which has been properly cited and referenced.

Signed by candidate

…….

Kirstin Petzer

……10 Feb 2023……

Date

Abstract

Due to global warming, Marine Heatwaves (MHWs) are considered to be one of the emerging threats to marine ecosystems globally. MHWs are prolonged periods of extreme warm Sea Surface Temperature (SST) anomalies which can cause severe ecological impacts by decreasing biodiversity, negatively affecting cold water species and increasing ocean stratification. Using the Cape Point CSIR half-hourly *in situ* SST, CCI, REMSS, ERA5 wind time series, over 17-years the occurrence from January 2003 to March 2020, duration and maximum SST values as well as the influence of the wind on the formation and end on marine heatwaves and warm events (WEs) at a single location in the Cape Peninsula Cell, in the Southern Benguela, was examined. The MHW events were identified using Hobday et al. (2016), when the SST exceeds the climatological 90th percentile for at least five days. The WE events, defined similarly to a MHW but the SST must exceed the climatological 90th percentile for at least three days, are also studied due to the high variability of the Southern Benguela. In the half-hourly CSIR time series 14 MHWs and 21 WEs occurred over the 17 years. The average duration is between 7 to 8 days but the longest events occurred during periods of decreased upwelling but the highest maximum SSTs occur during the periods of upwelling dominance. The daily CSIR, CCI and REMSS time series all identified double the number of MHWs and WEs events than the half-hourly time series, raising the concern of applying the Hobday et al. (2016) definition to sub-daily time series and the ability of satellites to be used for MHW identification in the Southern Benguela close to the coast. The dominant wind at the formation of MHWs and WEs is a north-westerly wind, indicating the main driver of events at the CSIR Cape Point mooring is the movement of warm water masses to the mooring location. The dominant wind direction at the end of the MHWs and WEs is a south-easterly wind indicating that coastal upwelling limits the duration of warm water events at the Cape Point mooring. Marine heatwaves are expected to worsen globally with climate change by lasting longer with high temperature increases but the projected increase in southeasterly winds could further limit the duration of MHWs in the Southern Benguela upwelling system.

Key words: Southern Benguela, marine heatwave, warm events

Table of Contents

Acknowledgments

This Master's Thesis would not have been possible without the people in my life who supported me in so many different ways. Just a few years ago I didn't know that I was capable of completing this type of dissertation, nevermind finding my love for coastal oceanography, research and even coding.

To my supervisors, thank you for guiding and teaching throughout these two years. To Tarron Lamont, thank you for always asking the hard questions and challenging me. I also want to thank you for being someone who I always thought I could talk to about my personal issues during this thesis. To the late Mathieu Rouault, thank you for all the opportunities you have given me. I will take the advice and all that you have taught me into my future work, rest in peace.

Thank you to everyone in the UCT Oceanography Department, with special mention to everyone in the Masters room, the Oceanography Postgraduate Committee and Mathieu's crew thank you for always offering a helping hand or sharing a laugh together. Thank you to EXEBUS for all your support. Thank you Serge, for helping me get access to data. To Riesna, thank you for being my rock during this thesis you have helped me in ways I can't even describe.

To my family, thank you so much for your endless support. Mom and Dad, thank you for always listening to my concerns and being there to motivate me. Lauren, thank you for being an amazing little sister and being with me when I needed a break.

List of abbreviations

CSIR - Council for Scientific and Industrial Research

CCI - Climate Change Initiative

REMSS - Remote Sensing Systems

GEBCO - General Bathymetric Chart of the Oceans

SAM - Southern Annular Mode

ENSO - El Niño–Southern Oscillation

ESA - European Space Agency

CDR - Climate Data Record

AVHRR - Advanced Very High Resolution Radiometer

ATSR - Along Track Scanning Radiometer

GHRSST - Group for High Resolution Sea Surface Temperature

MW_IR - Microwave and Infrared Radiometer

ECMWF - European Centre for Medium-Range Weather Forecasts

MHW – Marine Heatwave

BUS - Benguela Upwelling System

EBUS – Eastern Boundary Upwelling System

SAA - South Atlantic Anticyclone

SST - Sea Surface Temperatures

GDP - Gross Domestic Profit

MPA - Marine Protected Areas

ESACW - Eastern South Atlantic Central water

SACW - South Atlantic Central water

WE – Warm Events

List of Figures

Chapter 1 – Introduction and Key Questions

The Benguela Upwelling System (BUS) is situated off the west coast of southern Africa, in the South Atlantic Ocean (Hutchings, et al. 2009). Marine sectors in southern Africa coastal countries, such as fisheries and marine mining, depend on the BUS for economic growth (Kämpf & Chapman, 2016). In contrast to most other marine regions, the BUS is an Eastern Boundary Upwelling System (EBUS; Tim et al. 2018). Therefore, the fishing industries benefit from the high concentration of surface biological productivity in its coastal waters. The cold-nutrient rich waters that create the required conditions for intense productivity are forced to the surface by coastal upwelling. The coastal upwelling is driven by the strong coupling between atmospheric forcing and regional ocean circulation (Chavez & Messié, 2009).

One of the increasing threats to marine ecosystems in recent decades are Marine Heatwaves (MHWs, Holbrook et al., 2019). MHWs are prolonged periods of extreme Sea Surface Temperatures (SST) higher than the climatological (< 10 years) 90th percentile of SST, which have severe ecological impacts on the marine environment (Arafeh-Dalmau, 2019). Due to anthropogenic changes in the climate state, MHW days have increased in frequency on a global average by more than 50% per year (Oliver et al., 2018). Intense MHWs have the potential to affect marine ecosystems by decreasing biodiversity, negatively affecting cold water species, such as kelp, and increasing ocean stratification (Varela et al., 2021). One of impacts of ocean stratification, particularly on EBUSs, will be the inhibiting of upward mixing of water sources from below the euphotic zone. As a result of the stratification there will be a decrease in the supply of deep nutrients to the surface layer and will place a limit on biological productivity (Gupta et al., 2020).

As the Southern Benguela is not only important for South African economics but also the sustainability and adaptivity of small coastal communities, understanding the impact of extreme events on the Southern Benguela in the past, present and future is critical. One of the extreme events which has the potential to cause significant harm to marine environments is MHWs. The occurrence, characteristics, formation and dissipation of MHW in the Southern Benguela is still largely unknown and will be the focus of this thesis. Using the Council for Scientific and Industrial Research (CSIR) Cape Point mooring half-hourly *in situ* SST time series from January 2003 to March 2020 this study will have a fine temporal analysis of MHWs

within the Cape Peninsula Cell. This study will first answer the question, what are the characteristics of MHWs at the CSIR Cape Point mooring, such as MHW occurrence, duration and maximum temperatures? Secondly, how does the identification of MHWs differ between *in situ* half-hourly CSIR, *in situ* daily CSIR and daily satellite SST products? Thirdly, what is the influence of the wind on the formation and decay of MHWs at the CSIR Cape Point mooring?

Chapter 2 – Literature Review

2.1 Marine Heatwaves

Prolonged periods of anomalously warm SSTs can have significant impacts on the health of marine ecosystems and place a strain on marine biodiversity and by extension the regional fisheries economies (Holbrook et al., 2019). The concept of the intrusion of warm water disrupting the marine ecosystem is not a novel notion, in fact has been known for decades (Schlegel et al., 2019). The research into these warm water events intensified after the 1980's when the events became increasingly frequent and had larger impacts on the marine environment, but global observations were only confirmed in 2018 (Oliver et al., 2018). In order to estimate the impacts of the warm water events and allow for international comparison, in 2016 the extreme warm water events were labelled as 'marine heatwaves' (MHWs). Hobday et al. (2016) defines anomalously warm water events as MHWs if the SST values exceed the 90th percentile, based on a climatological record, for at least five consecutive days (Figure 2.1).

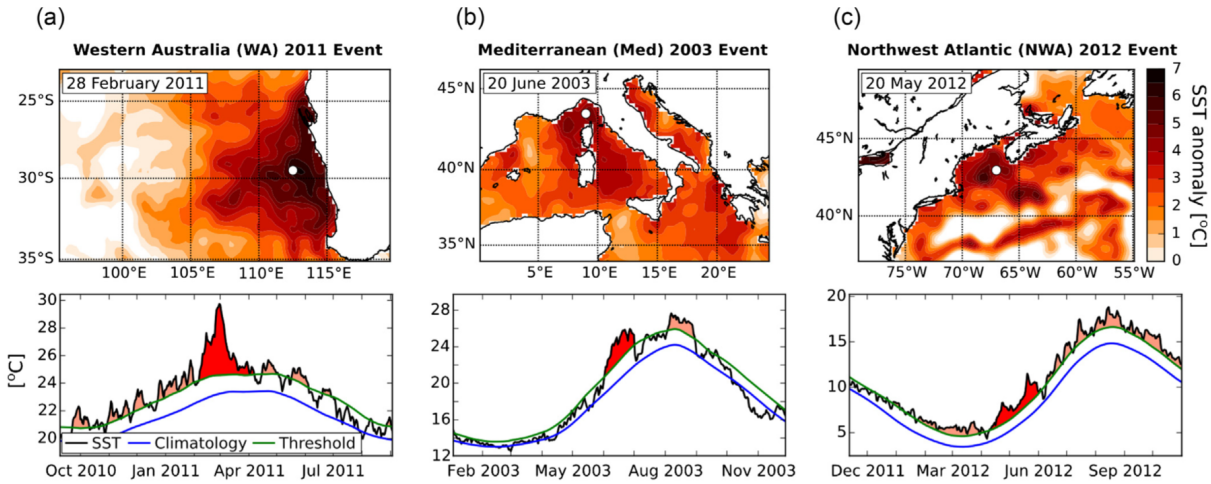

Figure 2.1: SST examples of MHW spatially (the first row) and over time (the second row) in A) Western Australia in 2011, B) Mediterranean in 2003 and C) the Northwest Atlantic in 2012 [Figure extracted from Hobday et al., 2016].

As the impacts of anthropogenic influence increase so does the impacts of MHWs. In fact, 87% of the MHWs can be attributed to human-induced global warming, mainly driven by anthropogenic greenhouse gases (Frölicher et al., 2018; Oliver et al., 2018). The immediate drivers of MHWs can be classified into three main categories. Gupta et al. (2020) states that (1) variations in the heat transport by the ocean (e.g. a boundary current intensification), (2)

coupled air-sea processes such as the El Niño–Southern Oscillation (ENSO) events and (3) persistent large-scale atmospheric synoptic systems are the three main categories. Prolonged MHWs have and will continue to cause irreversible negative impacts to biological marine systems (Schlegel et al., 2017). Socio-economic impacts can be caused by events such as toxic algae blooms, regime shifts in reef communities, mass coral bleaching and mass mortality of commercially central fish species during MHW events (Frölicher et al., 2018).

Marine biological systems are also affected by MHW's through the adjustment of physical oceanographic characteristics, other than the increase in temperature in the surface waters. Physical changes can include the vertical stratification of the surface waters which will inhibit upward mixing of nutrients to the surface or the mixing of phytoplankton downwards from the photic zone (Gupta et al., 2020). The strengthening of vertical stratification of the surface waters will have negative impacts particularly in EBUSs where it disrupts upwelling signals (Abrahams et al., 2021). The California Current System between 2014 and 2016 experienced an extreme warming event and is an example of the effects of a MHW on the marine environment in EBUSs (Arafeh-Dalmau, 2019). The duration and magnitude of the MHW was unprecedented and led to significant variations in the kelp bed community structure (Arafeh-Dalmau, 2019). After the MHW had subsided half of the invertebrate and fish species had disappeared. The warm waters also resulted in the introduction of algae species which were previously absent in the region (Arafeh-Dalmau, 2019).

2.2 Eastern Boundary Upwelling Systems

EBUSs are characterised by complex atmospheric, oceanic and biogeochemical dynamic processes that are not yet entirely understood. There are four EBUSs worldwide, the California Current System (along the North America west coast), Canary Current System (off northwest Africa), Humboldt Current System (off the coast of Peru and Chile) and the Benguela Current System (off southwestern Africa; Figure 2.2; Kämpf & Chapman, 2016). Due to the geographic placement of these regions and with respect to the atmospheric and oceanic conditions, together the EBUS's contribute about ±20% of the world's fish catches (Chavez & Messié, 2014). These systems are also significant when analysing the global ocean and climate models as they influence atmospheric circulation and heating which have feedback loops to large-scale climate systems. One of these coastal zones affected by the MHWs due to anthropogenic influence is the Benguela Upwelling system. The immense marine productivity of the Benguela, which stretches from Angola (15°) to the southern tip of South Africa's coastline (34°S), is essential

to the sustainability of Angola, Namibia and South Africa (Tim et al., 2018; Cochrane et al., 2009).

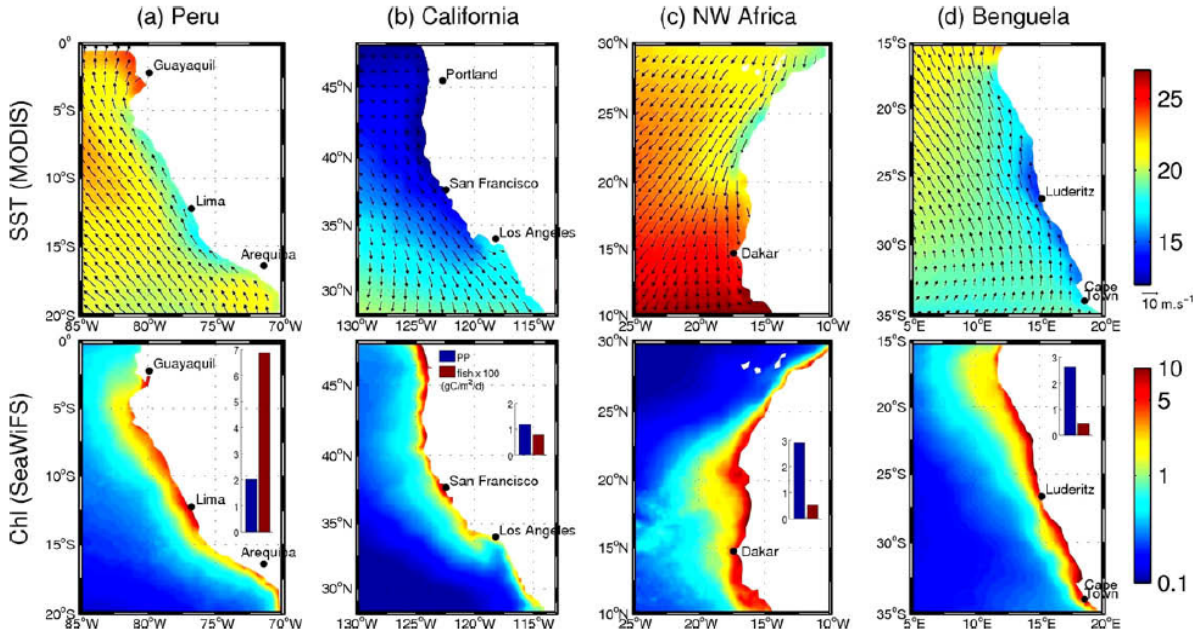

Figure 2.2: EBUS surface maps of SST (MODIS data) in the first row and chlorophyll (SeaWiFS) in the second row of A) Peru, B) California, C) Northwest Africa and D) Benguela [Figure extracted from Chavez & Messie, 2009].

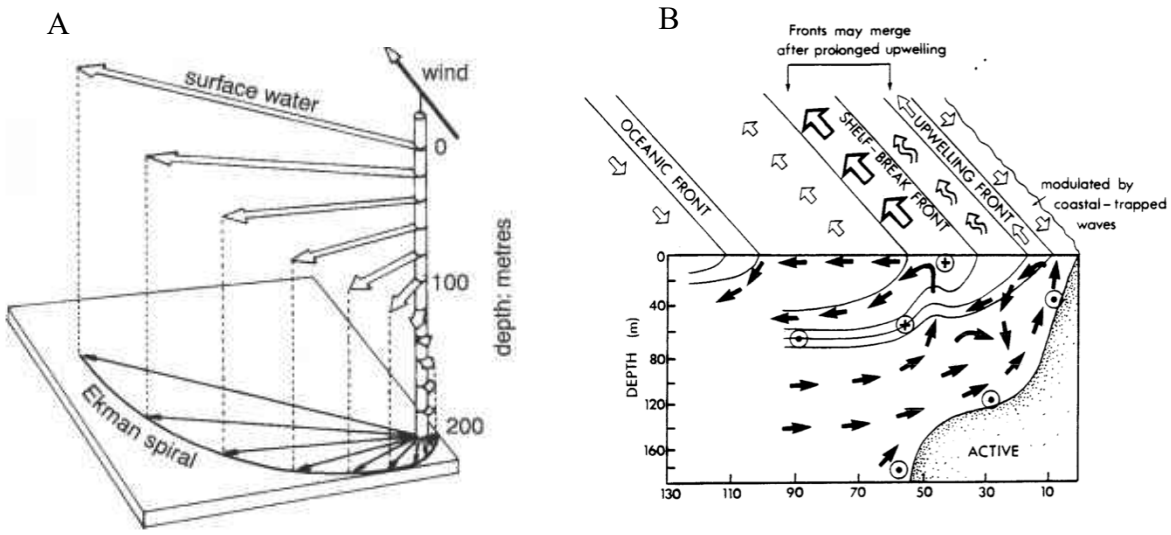

Figure 2.3: Diagrams of A) the Ekman spiral for the Southern Hemisphere and B) physical dynamics of coastal upwelling in the Benguela upwelling system [Figure extracted from Espinoza Morriberón et al., 2018 and Barange & Pillar 1992].

Upwelling refers to the movement of water masses upwards in the water column (Figure 2.3 Ding et al., 2021). While there are various processes which result in the upwelling of water,

the classification of upwelling which occurs in the Benguela (and the other EBUS) is coastal wind-driven upwelling (Kämpf & Chapman, 2016). In coastal upwelling the trigger of the upwelling is wind-induced offshore movement of the surface waters (Jacox et al., 2018). Wind stress and wind stress curl are induced from wind blowing over the ocean surface (which must blow parallel to the shoreline; Figure 2.3; Castelao & Barth, 2006). In combination with the rotational effects of the Earth and the associated Coriolis force, the effects of the wind stress change direction with depth, known as the Ekman spiral (Chu, 2015), resulting in the mass transport of the surface layer waters offshore. The horizontal divergence of the surface layer results in a vertical flux of water parcels in order to replenish the surface waters (Ding et al., 2020). This process is known as Ekman transport (Figure 2.3; Jacox et al., 2018). The water masses which are upwelled are generally cold and nutrient-rich and form the basis of the high biological productivity seen in EBUSs.

2.3 The Benguela Upwelling System

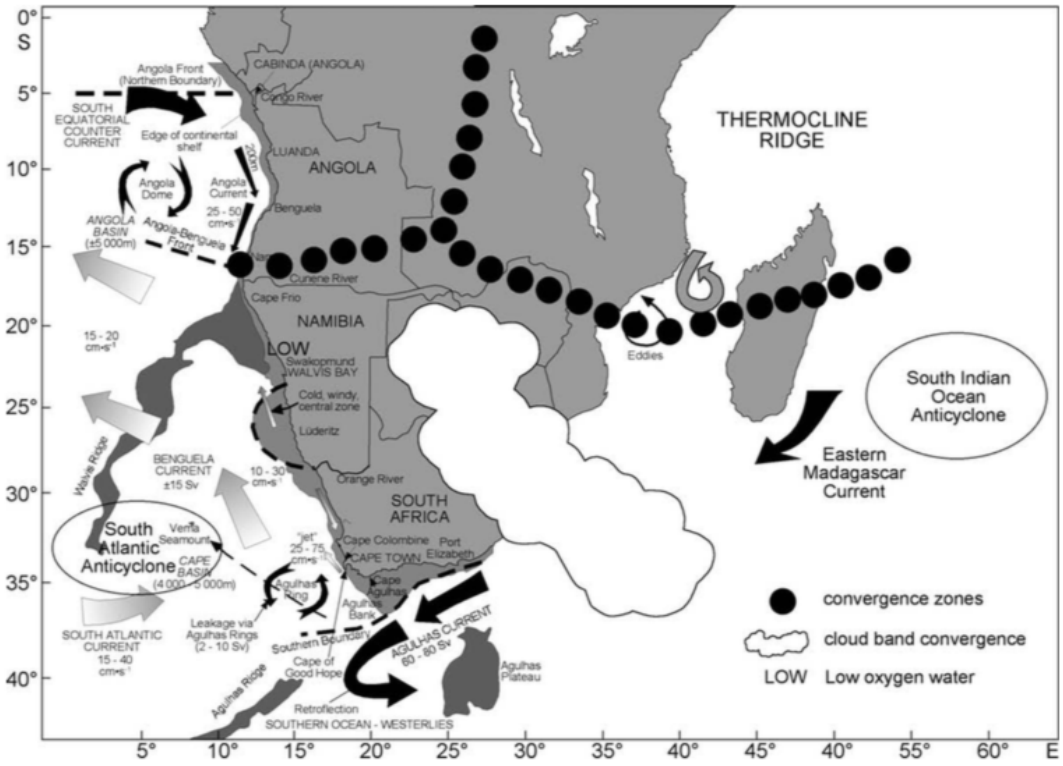

Figure 2.4: A spatial overview of the large-scale atmospheric and coastal oceanic features in the Benguela upwelling system [Figure extracted from Hutchings et al., 2009].

The BUS has unique oceanic physical characteristics, compared to the other EBUS, as it has two stratified warm or subtropical boundaries (Hutchings et al., 2009). The Benguela is

bounded in the north by the Angola-Benguela Front and in the southern region by the Agulhas Current (Hutchings et al., 2008). The upwelling regions are separated into the Northern and Southern Benguela mostly due to the different variation in upwelling between the three regions (Goubanova et al., 2013). The Northern Benguela is separated from the Southern Benguela by the Luderitz–Orange River Cone, a region of "strong winds, high turbulence and strong offshore transport" (Hutchings et al., 2009). The upwelling in the Northern Benguela is perennial, compared to the Southern Benguela which has seasonal upwelling. The coastal upwelling in the Benguela is wind-driven and the driving wind force in the Benguela is the South Atlantic Anticyclone (SAA) which has seasonal movement over the Southern Benguela (Figure 2.4; Shannon & Nelson, 1996).

The geographical placement of the BUS on the eastern boundary of the South Atlantic basin allows for the SAA (Figure 2.4) to generate south-easterly winds over the region. The south-easterly winds blow parallel to the Southern African coastline and as stated by Kruger et al. (2009) when winds flow parallel to a barrier the surface waters will be transported off the coast of southwest Africa. The coastal upwelling process provides a basis for the high biological productivity which multiple industries depend on along the southwest Africa coast (Kämpf & Chapman, 2016). Marine tourism, commercial and small-scale fisheries are some of the most widespread uses of the Benguela upwelling system which contribute significantly to the South African, Namibian and Angolan Gross Domestic Profit (GDP; Finke et al., 2020). While the Benguela Upwelling system is economically significant it is also biologically noteworthy. Throughout the Benguela 18 Marine Protected Areas (MPA) 17 which are located in the South African Benguela sector have been identified as areas of high conservation importance (Finke et al., 2020).

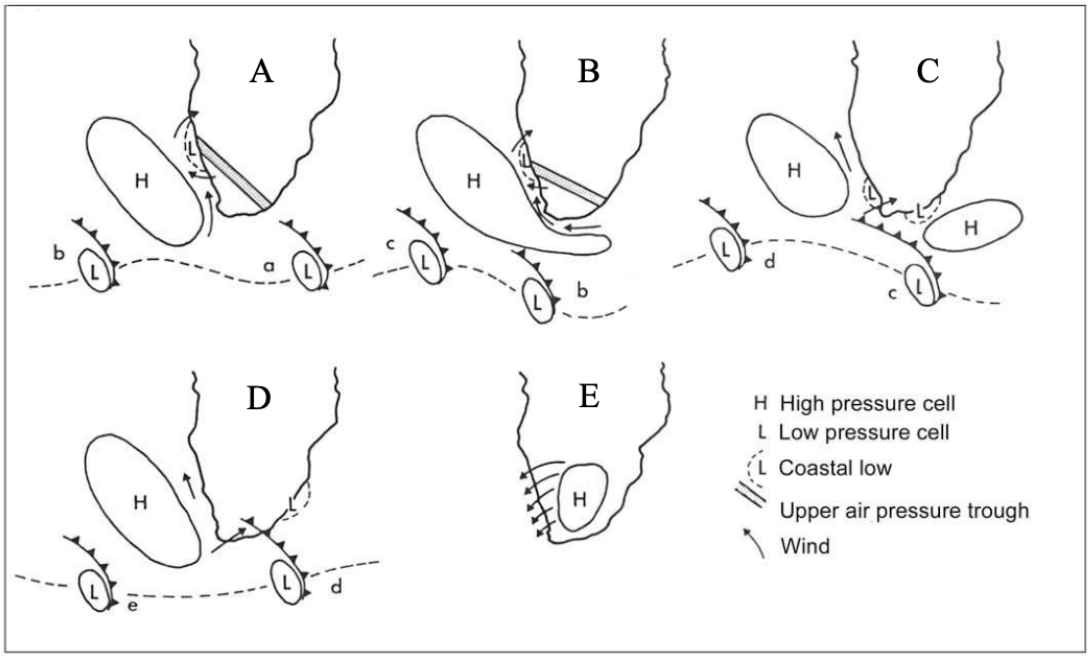

Figure 2.5: A diagram indicating the direction of wind over the Southern Benguela by the placement and interaction of the high (H) and low (L) pressure cells [Figure extracted from Flynn et al., 2019 (modified from Nelson and Hutchings, 1983)].

2.3.1 Southern Benguela characteristics and variability

In the Southern Benguela, the SAA is responsible for generating upwelling favourable south-easterly winds along the southwest Africa coastline during the austral summer (Figure 2.5A; Shannon & Nelson, 1996; Jacox et al., 2018). Due to the dominance of upwelling favourable winds in the summer and spring, there is a noticeable temperature gradient between inshore, reaching as low as 9°C, and offshore, reaching ±22°C (Weeks et al., 2006; Whittle et al., 2008). As the latitude of the most intense input of solar radiation shifts northward in the austral winter, so does SAA and the west wind belt which forms cyclones moving eastward (Hutchings et al., 2009, Siegfried et al., 2019). During the austral winter the cyclonic weather systems create a dominance of north-westerly winds over the Southern Benguela (Andrews & Hutchings, 1980). In the austral summer the effect of the low pressure cells, associated with cyclonic air rotation, is weak. The duration of the south-easterly winds are modulated in periods between 3-10 days, when there will be wind relaxation or a passage of cyclones south of Southern Africa inducing a wind reversal (Shannon and Nelson, 1996).

There are other large-scale atmospheric processes which affect the upwelling in the Southern Benguela such as the ENSO (Tim et al., 2015). ENSO refers to the year-to-year fluctuation of El Niño and La Niña conditions. El Niño events are characterised by the warming of the tropical Pacific Ocean surface waters and the weaking of the equatorial trade winds (Timmermann et al., 2018), while the conditions during La Niña events are the reverse to normal conditions of El Niño conditions. The impacts of ENSO on atmospheric dynamic fields are seen worldwide. As the SAA shifts poleward during La Niña, there is an increase in the dominance of upwelling favourable south-easterly winds over the Southern Benguela (Philippon et al., 2012; Dufois & Rouault , 2012). During El Niño there is an increase in north-westerly wind anomalies as a result of the equatorward movement of the SAA allowing for cold-front and cut-off lows to be pass over the Benguela EBUS (Philippon et al., 2012; Dufois & Rouault , 2012).

The upwelling is not homogeneous throughout the BUS with upwelling cells of various intensity alternating sometimes with retention zones. Throughout the Benguela there are seven centres of intense upwelling (Hutchings et al., 2009). The position of the centres of upwelling are determined not only by locally enhanced wind stress curl but also by changes in the orientation of the coastline (coastal topography and shelf depth) and are defined as upwelling cells (Shannon & Nelson, 1996; Hutchings et al., 2009). The upwelling cell which is seen as a separator of the Northern and the Southern Benguela regions is the Lüderitz upwelling cell at 26°S (Figure 2.6; Ekau et al., 2010). The Lüderitz upwelling cell is the most energetic cell and behaves as a barrier restricting the transport of energy, nutrients and water masses (Hutchings et al., 2009) The three upwelling cells in the Southern Benguela are the Cape Peninsula cell, Columbine cell and Namaqua cell (off the coast of the Cape Peninsula, Cape Columbine and Hondeklip Bay; Figure 2.6; Nelson et al., 1983).

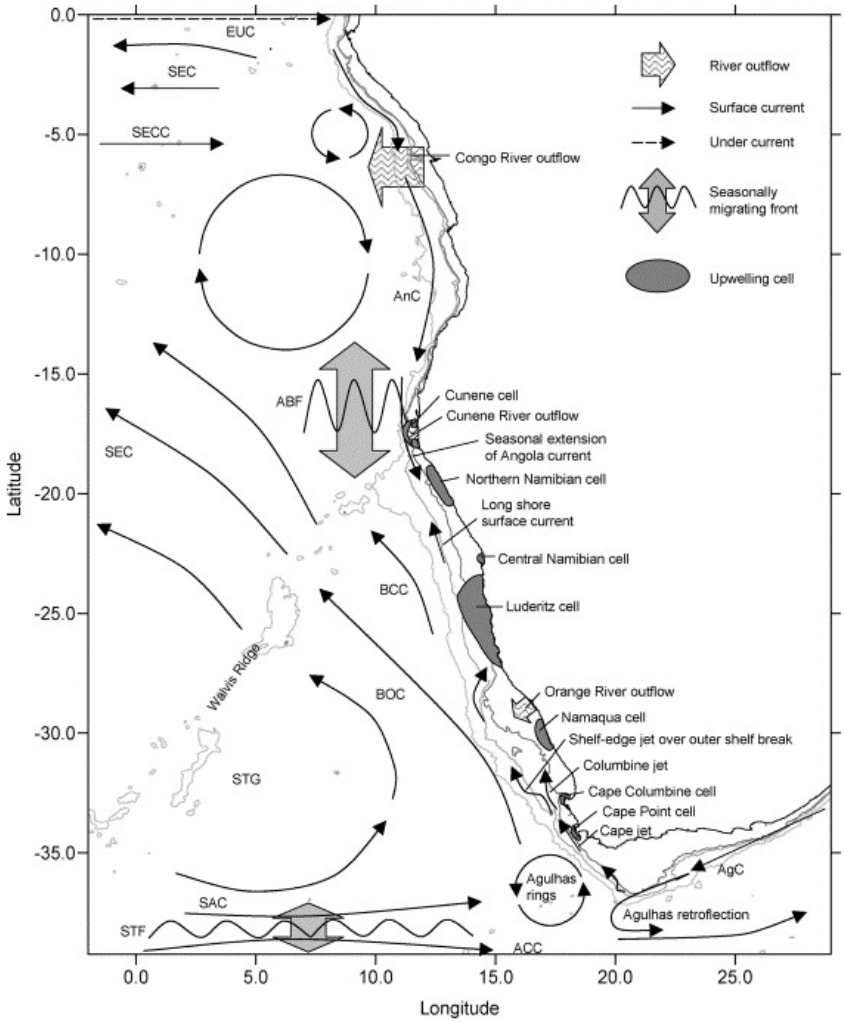

Figure 2.6: Diagram of the Benguela Upwelling system indicating the placement of upwelling cells and the movement of frontal jets, currents, Agulhas retroflection and leakage [Figure extracted from Hardman-Mountford et al. (2003)].

While the Southern Benguela is characterised by “a pulsed, seasonal, wind-driven upwelling at discrete centres" another key component to the productivity of the Southern Benguela is the water masses which are upwelled to the surface (Hutchings et al., 2009). The cold-nutrient waters permit for the presence of cold-water species and the prosperity of these species through the supply of nutrients such as phosphate and nitrate (Seabra et al. 2019; Carr & Kearns, 2003). The concentration of nutrients supplied to the Benguela is determined by the source waters, which in the Southern Benguela is predominantly the Eastern South Atlantic Central water (ESACW; Figure 2.4; Tim et al., 2018). ESACW is formed in the Cape basin Region where Agulhas leakage mixes with South Atlantic Central water (SACW; Figure 2.4) sourced from the Brazil-Malvinas Confluence Zone (Tim et al., 2018). The ESACW is more saline than the SACW from mixing with the ‘younger’-high saline waters from the Agulhas Current

(Mohrholz et al., 2008). The high saline Agulhas leakage is also a source of oxygen-rich water into the South Atlantic basin (Liu & Tanhua, 2019).

The Benguela Current is a key component to understanding the Southern Benguela circulation (Figure 2.4; Garzoli & Gordon, 1996). The current is generated from the physical effects of the wind stress curl but in the south it is also driven by "non-linear interactions of passing Agulhas rings" (Veitch et al., 2010). The Benguela current is a shallow, broad current which transports 15 Sv northward at a rate of 10-30 cm s^{-1} (Shannon ,1985). In the Southern Benguela the Benguela Current is characterised by two main flow paths moving equatorward, the Benguela Oceanic Current and the Benguela Coastal Current (Hardman-Mountford et al., 2003). The Benguela Oceanic Current is the segment of the current that is positioned in the Agulhas eddy corridor and is driven by the Oceanic Front (Figure 2.7A). The Oceanic Front separates the warmer South Atlantic subtropical gyre offshore waters from the cool, inshore coastal waters from the upwelling region (Garzoli & Gordon, 1996).

Due to the proximity of the Southern Benguela to the Agulhas Current (Figure 2.6), the mixing of Agulhas waters with SACW to create upwelling source waters is not the only intrusion of the warm saline water into the Benguela (Tim et al., 2018). The Agulhas Current is a Western Boundary Current along Southern Africa in the South Indian Ocean sourcing high salinity waters (Lutjeharms et al., 1988). While 90% of the Agulhas retroflection water mass transport is returned to the South Indian Ocean (Figure 2.4) the remaining 10% is transported into the South Atlantic (Whittle et al., 2008). The intrusion of the warm saline water is crucial for inter-basin salt and heat exchange and forms a key role in the global thermohaline circulation pattern (Whittle et al., 2008; Veitch & Penven, 2016).

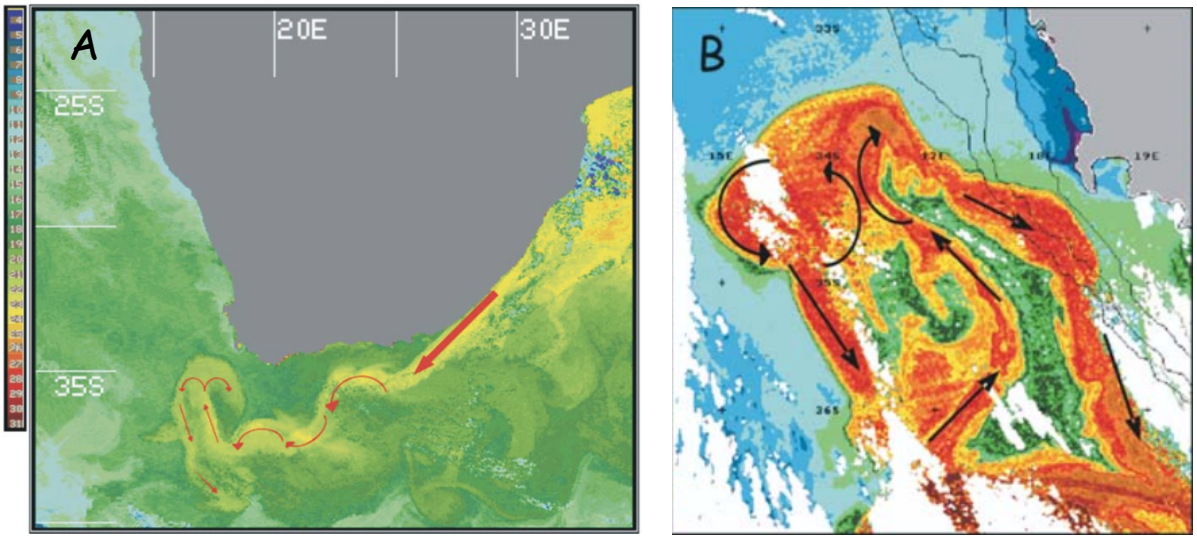

Figure 2.7: A) RSMAS SST (°C) map of Benguela upwelling system, the Agulhas Current and leakage region on the 9th of December 1996. B) RSMAS SST (°C) map of Cape Peninsula Cell (Southern Benguela) region on the 13th of December 1996. Arrows indicate the direction of flow [Figure extracted from Whittle et al., 2008].

The large Agulhas rings and eddies which shed off the retroflection into the South Atlantic merge with the Benguela Current (Figure 2.6; Veitch, 2010). A smaller contributing component to the transport of Agulhas water is by the advection of filaments off the retroflection into the Benguela region, as seen in the case study (Figure 2.7) done by Whittle et al. (2008). The intrusion of the warm water, corresponding to increased westerly winds, through rings and filaments have been proven to interact with the upwelling system and influence biological processes on the shelf (Hardman-Mountford et al., 2003; Duncombe Rae et al., 1992a, 1992b).

2.4 Marine Heatwaves in the Benguela Upwelling System

The direct and indirect effects which MHWs will have on upwelling and the marine ecosystem in the Southern Benguela are yet to be fully understood. According to Gupta et al. (2020) the most intense MHW events occur in summer, which will be partially impactful in the Southern Benguela, as its seasonal upwelling occurs in the austral summer. The influx of warm water into the coastal upwelling system can lead to nutrient-depleted surface waters due to a weakening of coastal upwelling through thermal stratification (Schiel & Foster, 2015; Arafeh-Dalmau et al., 2019). Varela et al. (2020) poses that upwelling can be considered as a physical oceanic moderator for the occurrence and duration of MHWs. As the variation in wind in the Southern Benguela has cycles of 3-10 days followed by either a reversal or relaxation of wind, the wind may be a driver of the decay of MHWs (Shannon and Nelson, 1996).

The absence of upwelling favourable wind may also be the instigator of MHWs, as low (or no) wind periods can lead to warming of surface waters (Gupta et al., 2020). In the case of the Southern Benguela strong north-westerly/westerly wind, may drive warm water (up to 22°C) from offshore into the coastal upwelling region (Weeks et al., 2006; Whittle et al., 2008). The waters offshore have an observed range extending to 22°C due to the Southern Benguela's proximity to the mixing of Agulhas waters with South Atlantic surface waters (Tim et al., 2018). Another possible formation of MHWs in the Southern Benguela is the intrusion of Agulhas features such as filaments which will particularly affect the Cape Peninsula upwelling cell, as it is the most southern upwelling cell (Figure 2.7; Figure 2.6; Whittle et al., 2008). While upwelling ecosystems systems have rapid changes in SST, the pressure that MHWs place on species (particularly cold-water species which are adapted to upwelling zones) is noteworthy and therefore their frequency, duration and drivers are important to understand in the Southern Benguela (Seabra et al. 2019; Arafeh-Dalmau et al., 2019).

Chapter 3 – Data and Methods

This chapter describes the data and methods used to address the research objectives outlined in the prior chapters. In the first section the CSIR, Climate Change Initiative (CCI) and Remote Sensing Systems (REMSS) SST datasets are described. The CSIR SST dataset is used to identify and determine the characteristics of MHWs at the CSIR mooring, seen in Figure 3.1. The CCI and REMSS SST datasets are used to describe and examine the changes in SST in the Southern Benguela and the spatial formation of MHWs. The second section describes the ERA5 wind product and explains the methods used to analyse the wind's influence on the build-up and decay of both MHW .

3.1 Study domain

Figure 3.1 shows the CSIR Cape Point mooring where the MHWs will be identified and discussed. The region in which the ERA5 reanalysis data was extracted can also be seen in Figure 3.1 by the black square.

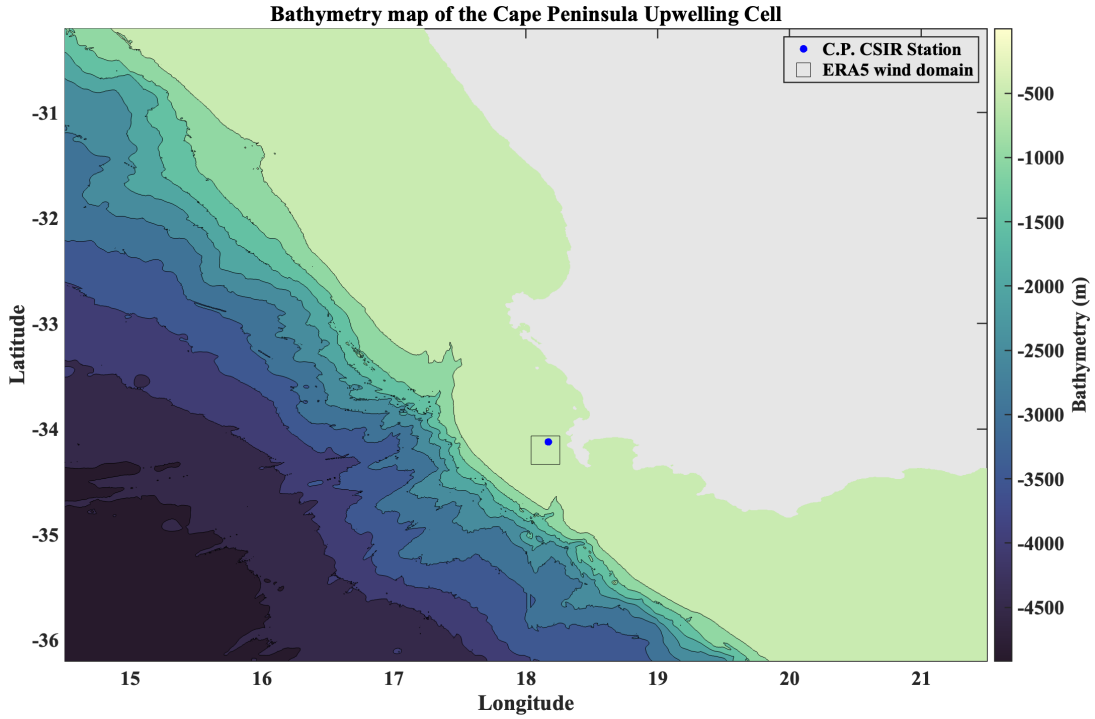

Figure 3.1: A bathymetry map of the Southern Benguela Upwelling system using General Bathymetric Chart of the Oceans (GEBCO) product (GEBCO, 2022). The bathymetry contours in the map are in increments of 500m. The blue data point indicates the location of the CSIR Waverider buoy and the black box surrounding the blue data point represents the domain of the ERA5 wind data.

3.2 Sea Surface Data sets: Product Information

3.2.A. CSIR Cape Point SST

The CSIR is a South African organisation which contributes to the socio-economic prosperity of South Africa through the development of scientific and technological research (CSIR, 2021). Datawell Waverider buoys were installed in order to record and statistically analyse the coastal oceanic conditions along the South African coastline (Wavenet, 2021). At first the accelerometer Datawell Waverider buoys were deployed to collect wave height data (Wavenet, 2021). Recently, the moored wave buoys monitor and collect real time ocean wave and weather time series. The product time series include wave height, wave direction, SST (near the ocean surface), wind speed and direction (Wavenet, 2021). For the purpose of the study the Cape Point SST time series was analysed as an initial signal for MHW the Southern Benguela. These time series have also been used by Veitch et al. (2019) who used the Cape Point products to investigate how extreme wave events are influenced by the Southern Annular Mode (SAM) and ENSO.

The SST Cape Point Datawell Waverider time series used in this study is from January 2003 to March 2020. Schlegel et al. (2019) states that in order to study MHWs a time series of at least 10 years must be used. As the Cape Point SST time series has a temporal scale of every half hour, this allows for fine temporal exploration of SST as a proxy for MHWs. The Cape Point buoy is located 34°12'14.40"S, 18°17'12.01"E, approximately 5.4 km off the coast of Cape Point (Wavenet, 2021).

3.2.B. CCI Satellite SST

The Climate Change Initiative Sea Surface Temperature project (SST_CCI) was produced by the European Space Agency (ESA) who have produced v2.1 SST_CCI Level 4 Climate Data Record (CDR; Tsamalis & Saunders, 2018). The SST dataset is produced by combining data from both Advanced Very High Resolution Radiometer (AVHRR) as well as Along Track Scanning Radiometer (ATSR) SST_CCI CDRs (Merchant et al., 2014). The CDRs were combined using a data assimilation method to produce SST values for areas which lack values. Due to the data assimilation the CCI dataset is able to produce a globally complete daily SST analysis with a 0.05°x0.05° spatial resolution (Bulgin et al., 2016). The CCI SST product has data available from 1981 to the present and has been adjusted for the standard local time

between 10:30/22:30. The data set can be used for model evaluations of climate and ocean processes, quantifying changes in the marine environment and detecting marine variability, such as MHWs (Merchant et al., 2019).

3.2.C. REMSS Satellite SST

The Group for High Resolution Sea Surface Temperature (GHRSST) global Level 4 analysis dataset was produced by the REMSS (NASA, 2023). The Optimally Interpolated SST dataset uses Microwave and Infrared Radiometer data (MW_IR; e.g. MODIS; Remote sensing system, 2023). The product combines the microwave data for its through-cloud capabilities and the infrared data as it has high spatial resolution and also has the capability to go near the coast. A diurnal model was used to adjust the SST values to optimally make use of daytime retrievals to produce a foundation SST. The SST product is at a daily temporal resolution with a 9 km spatial resolution from 2002-06-01 to the present. The MW_IR SST dataset has been used in studies researching oceanographic parameters such as altimeter-derived surface currents, eddies influence on cyclone intensity and oceanic rain rate estimates (Ciani et al., 2020; Ali et al., 2007; Ahmad et al., 2005).

3.2 SST Methods

3.2 A. MHW and Warm Event (WE) definition

Some studies, such as Sorte et al. (2010), adopted previously used atmospheric metrics to understand and assess thermal stress in the marine environment. Sorte et al. (2010) defined MHWs as an event which lasts between three to five days and which have a mean/maximum temperature anomalies that deviate from the long-term mean by at least 3°C to 5°C. Other metrics used to define MHWs have been thermal stress anomalies (TSAs) and SST percentile thresholds (Selig et al., 2010; Marbà et al., 2015). In this study the definition of MHWs used will be the definition proposed by Hobday et al. (2016) MHW definition. Anomalously warm water events are defined as a MHW if the SST values exceed the climatological 90th percentile for at least five days continuously.

Hobday et al. (2016) states that the reason for using a 5-day criteria for the MHWs definition is that the 3-day limit criteria lead to the identification of many MHWs, mostly in the tropical regions, which wasn't ideal for a global comparison definition. Given the high variability in the Southern Benguela, particularly at sub-daily time scales, extreme warm water events could

be overlooked. Another potential concern is that when using datasets other than that at daily timescales, which Hobday et al. (2016) uses, it may change the number of MHWs identified. For example, MHWs identified from half-hourly observations may not exist in daily time series, since the half-hourly SSTs above the 90th percentile could be averaged out at the daily time scale. Therefore, this study will also identify and observe Warm Events (WEs) which will be defined as SST values exceeding the climatological 90th percentile for at least 3 days continuously.

Hobday et al. (2016) defines a MHW event as 'discrete', as an event which has a well-defined beginning and end to an event. However, MHW defined events with a gap of two days or less are defined as one MHW. An example will be two events, one event with five anomalously warm days and one with seven anomalously warm days separated by two cooler days [5_{hot}, 2_{cold}, 7_{hot}], the event would be defined as a 14 day event. The definition of WEs for this study, will also follow the Hobday et al. (2016) definition of a MHW but if between them, they have a period of SST lower than the climatological 90th percentile for less than 24 hours it will be defined as a single WE.

3.2 B. Climatologies

The CSIR monthly climatology was calculated, in MATLAB, by averaging all the data points per month over 17-years from January 2003 to March 2020. The daily CSIR dataset is created by averaging each day's half-hourly values into a single daily data point to facilitate comparison with satellite remote sensing. The monthly CCI, REMSS SST climatologies are calculated using the same method as the CSIR monthly climatology but with a daily time step. In order to identify the extreme warm water events in the half-hourly CSIR, daily CSIR, CCI, REMSS SST time series of each of their 90th percentile climatologies are calculated. All 90th percentiles were smoothed using a 30-day 'moving window' as suggested by Hobday et al. (2016). The SST climatological mean, 1 standard deviation, 2 standard deviation and 90th percentile were all calculated in MATLAB using built-in functions.

3.4 Wind Datasets: Product Information

3.4.A. ERA5 Wind

The ERA5 is a fifth generation European Centre for Medium-Range Weather Forecasts

(ECMWF) reanalysis which provides hourly estimates of ocean-wave, atmospheric and land-surface climate quantities (Copernicus, 2021). The ERA5 reanalysis is generated using 4D-Var data assimilation and model forecasts combined with observations worldwide. ERA5 atmospheric products include potential vorticity, fraction of cloud cover and the U-component and V-component of wind. The ERA5 U-component and V-component of wind will be used in this study as it was also used by Abrahams et al. (2021) to analyse variation and change of upwelling dynamics in Eastern Boundary Upwelling Systems, including the Benguela Upwelling System.

For the purpose of this study a subset of the ERA5 U-component and V-component of the wind dataset is extracted over the 34°25'S, 18°50'E region. The time series lasts from January 2003 until December 2019 and has an hourly temporal resolution and 0.25°x0.25° spatial resolution at the surface level. The U and V components are the vector components of the wind speed and wind direction. The U component represents the zonal component of the wind. The positive U component values denote westerly wind (wind movement from the west to east) and negative U component values denote an easterly wind (wind movement from the east to west). The V component represents the meridional component of the wind. The positive V component values denote a southerly wind (wind movement from the south to the north) and negative V component values denote a northerly wind (wind movement from the north to the south).

3.5 Wind Methods

The ERA5 V and U wind monthly climatology was calculated in MATLAB, by averaging all the U and V wind data points per month over 17-years from January 2003 to March 2020. The ERA5 U and V wind product was also used to record the dominant wind direction on the day of the onset, and the end, of each MHW and WE event.

Chapter 4 – Results

This section will first look at the monthly CSIR SST and ERA5 wind climatologies at the CSIR mooring station. Next, the characteristics of MHWs and WEs in the CSIR time series will be described through the occurrence, duration and maximum temperatures at the CSIR mooring. This section will also do a comparison of the identification of MHWs and WEs in the half-hourly CSIR, daily CSIR, daily CCI and daily REMSS datasets. Lastly, the formation and dissipation of MHWs and WEs at the CSIR mooring will be described with the use of ERA5 wind dataset and CCI anomaly maps.

4.1 Climatologies for CSIR SST and ERA5 wind

In this subsection, the monthly CSIR SST and wind climatologies at the CSIR mooring station will be described. This will be to identify the periods of upwelling and non-upwelling which will affect the movement of the surface waters where the MHWs and WEs will be identified.

Figure 4.1 A shows the climatological annual cycle of SST at the CSIR mooring station in the Cape Peninsula cell using half-hourly values over 17 years from 2003 to 2020. The annual cycle shows SST values below 13.5°C for the months between October through to April (Figure 4.1 A). The monthly averages between May and September show higher SST values between 14°C and 15°C.

Figure 4.1 B shows the hourly and monthly climatology of the U and V wind speed components from ERA5 data at the CSIR mooring. In between October to the end of April the wind has a dominance of south-easterly winds, positive V and negative U wind (Figure 4.1 B). Between May to the end of September the wind has a dominance of north-westerly winds, negative V and positive U wind (Figure 4.1 B). The shift in wind direction dominance aligns with the shift of SST values (Figure 4.1 A). The wind in the upwelling season, October to March, is stronger than the non-upwelling season. The upwelling season has average V wind speeds between 3 m s^{-1} to 5 m s^{-1} and average U wind speeds between -1.5 m s^{-1} to 3 m s^{-1} (Figure 4.1 B). The non-upwelling season has average V wind speeds between -1 m s^{-1} to 3 m s^{-1} and average U wind speeds between -2 m s^{-1} to 1 m s^{-1} (Figure 4.1 B). Therefore, not only does the wind regime shift but there are also stronger wind speeds in the upwelling season.

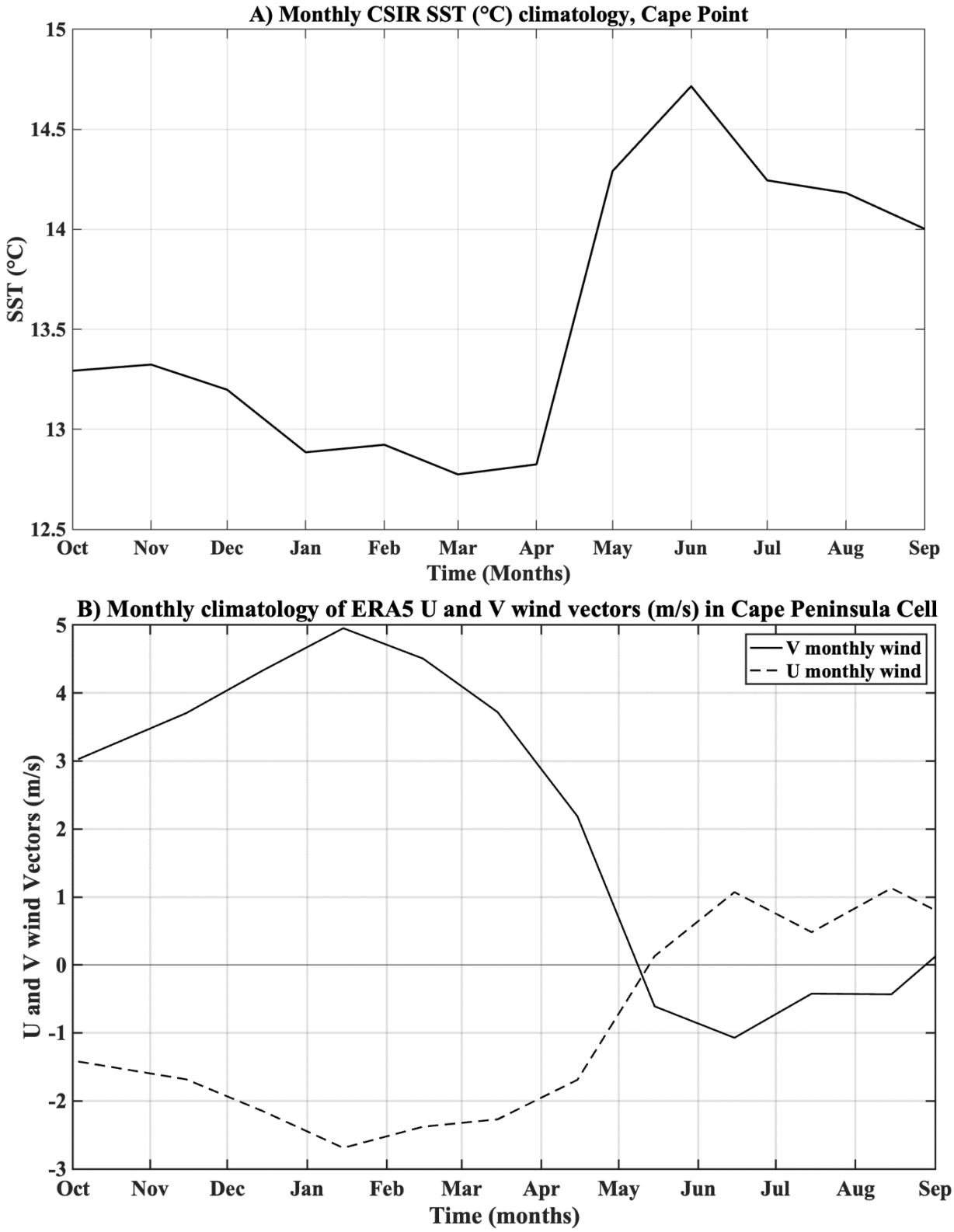

Figure 4.1: Monthly climatological time series between 2003 to March 2020 from October to September of A) CSIR SST Cape Point data and B) ERA5 monthly V (solid black) and U (dashed black) wind speed component at the CSIR mooring site.

As austral summer months are known as an upwelling period compared to the winter months which are not seen as an upwelling period, in order to understand the influence of upwelling on the characteristics of MHWs and WEs, these seasons will be separated. The year will be separated into two six month seasons, the upwelling season (from October to March) and the non-upwelling season (from April to September). While April has a SST monthly climatological value closer to the upwelling season and has south-easterly winds (Figure 4.1), this study will not be including April in the upwelling season. As the SAA reaches the northern extremity around May, during April the SAA is shifting equatorward which can be seen in the climatology with a decrease in south-easterly winds (Figure 4.1 B). Also, as SST can be used as an identification of upwelling events it is also affected by solar radiation and in autumn the solar radiation decreases which could be increasing the influence of the upwelling which occurs compared to the summer months (Figure 4.1 A).

4.2 CSIR mooring MHW characteristics

In this subsection, the full CSIR time series is plotted with the 10^{th} and 90^{th} SSTs as well as the climatological CSIR SST 1^{st} and 2^{nd} standard deviation. In the CSIR full time series, the MHWs and WEs are also plotted to have a temporal understanding of the frequency of the warm water events. The total number of MHWs and WEs identified in the CSIR SST Cape Point mooring time series from 2003 to March 2020 will be listed. In order to have a visual understanding of the distribution of the number of CSIR MHWs and WEs days and their maximum SST values, histograms of Table 4.1 are also shown.

In Figure 4.2 the full SST time series at the CSIR mooring can be seen as well as the annual climatology of 1 and 2 standard deviations. The occurrence of SST values above the 90^{th} percentile and below the 10^{th} percentile can also be seen, along with the visual distribution of MHWs and WEs over a 17 year period. Periods of SST above the 90^{th} percentile (the brown SST time series) that do not meet the classification of SST values above the 90^{th} percentile for at least three days, are defined as heat spikes (Figure 4.2). It is also worth noting that there are large breaks in the SST time series during the years of 2008, 2009, 2018 and 2019 Therefore, the account of MHWs and WEs could be slightly different if the time series was complete.

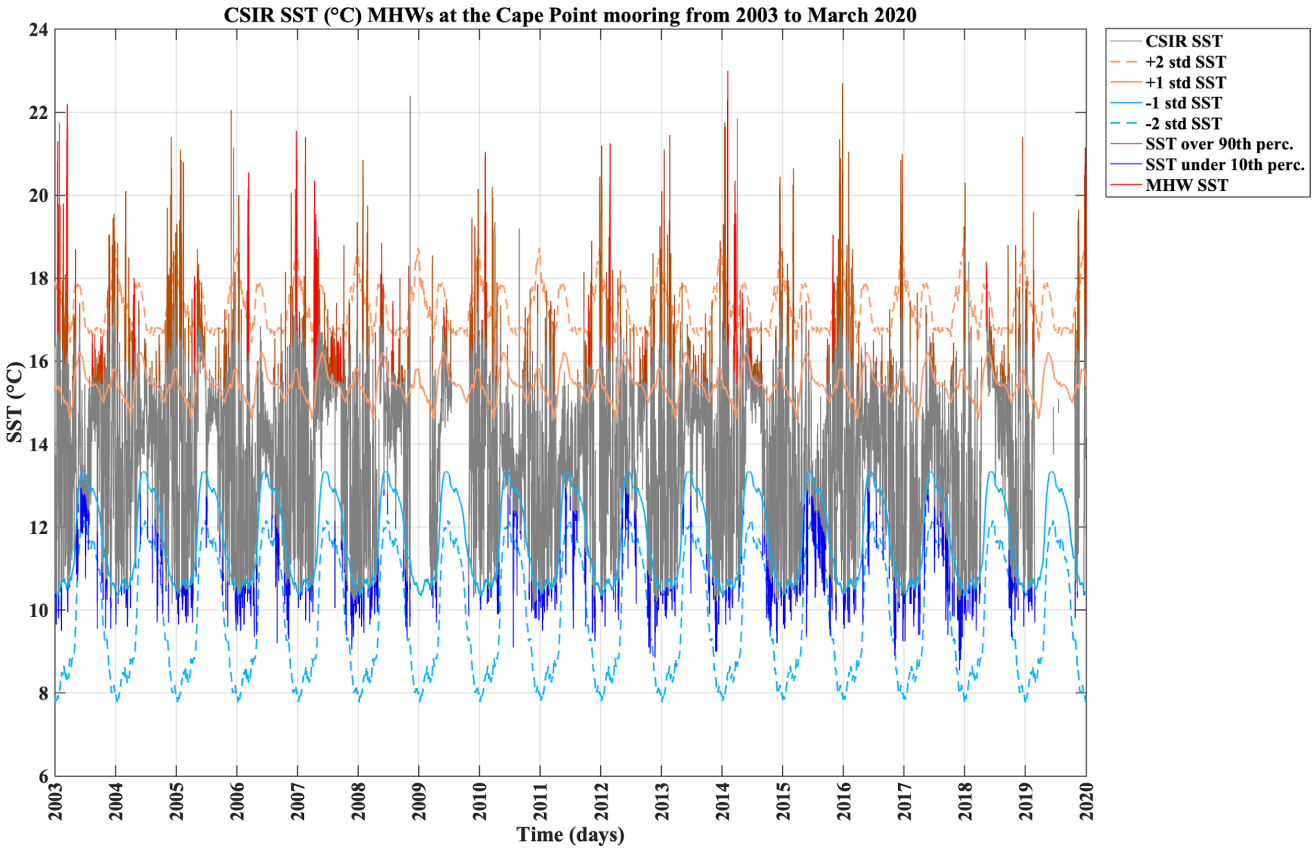

Figure 4.2: CSIR SST (°C) from 2003 to March 2020, at Cape Point CSIR station. The original CSIR SST time series (grey), +2 standard deviation (dashed orange), +1 standard deviation (orange), -1 standard deviation (light blue), -2 standard deviation (dashed light blue), above the 90th percentile CSIR SST (brown), under the 10th percentile CSIR SST (dark blue), CSIR SST defined MHWs and WEs (red) of CSIR SST is plotted.

The 1 standard deviation ranges between 16.19°C in May and 14.67°C in March (Figure 4.2). In between the two range values the SST decreases from May to 15.4°C in October and then increases to 15.8°C in December, then the SST decreases until March. The 2 standard deviations range between 16.8°C from July to October in May, and 18.66°C in January (Figure 4.2). In between the two range values the SST decreases from January to 16.55°C in March and then increases to 17.89°C in May when the SST decreases until July. The influence of the solar radiation is apparent in the 1 and 2 standard deviation SST values in summer. A few of the MHWs and WEs have SST values between 1 and 2 standard deviations, partially in winter, and therefore are within natural SST variations. The MHWs and WEs which are above 2 standard deviations are observed to occur more frequently in the upwelling season. There are also many examples of SST above the 90th percentile higher than 2 standard deviations, therefore not included in the natural variability but also not classified as a MHWs or a WEs.

No.	Event dates	Event Type	Total Length of event (# of days)	Max. SST (°C)
1	15 - 22 Jan 2003	MHW	8	21,3
2	13 - 18 Mar 2003	MHW	6	22,2
3	14 - 18 Aug 2003	WE	3	16.63
4	18 - 26 April 2004	MHW	9	18
5	27 Jan - 04 Feb 2005	WE	9	21,1
6	20 - 27 April 2005	MHW	6	18,05
7	9 - 12 May 2005	WE	3	18,7
8	16 - 25 May 2005	WE	10	18,3
9	10 - 16 Mar 2006	MHW	7	20,55
10	25 Dec - 01 Jan 2006	WE	8	21,55
11	13 - 18 Apr 2007	MHW	6	20,35
12	22 Apr - 04 May 2007	MHW	13	19,55
13	24 Jul - 06 Aug 2007	MHW	15	16,85
14	11 - 17 Aug 2007	WE	7	16,55
15	01 - 24 Sep 2007	MHW	25	16,6
16	25 - 30 May 2008	WE	6	18,85
17	30 Jul - 03 Aug 2007	MHW	5	17,45
18	04 - 08 Jun 2009	WE	3	17.3
19	07 - 13 Feb 2010	WE	7	21,05
20	24 - 30 Mar 2010	WE	7	20,15
21	20 - 25 Oct 2010	WE	6	17,05
22	31 Mar - 04 Apr 2011	WE	5	17,25
23	25 Oct - 01 Nov 2011	MHW	8	17,6
24	07 - 15 Nov 2011	WE	10	18,9

Table 4.1: A table describing characteristics of the MHW events at the CSIR Cape point mooring from January 2003 to March 2020. Characteristics include MHW event start and end date, if the event is a MHW or a WE, length of the MHWs and maximum SST (°C) during the MHW events.

No.	Event dates	Event Type	Total Length of event (# of days)	Max. SST (°C)
25	26 Feb - 05 Mar 2012	WE	9	21,25
26	30 Sep - 06 Oct 2012	WE	7	16,85
27	08 Feb - 13 Feb 2014	WE	6	23
28	25 Mar - 04 Apr 2014	MHW	11	20,35
29	09 - 12 May 2014	WE	3	17.65
30	25 - 30 Jun 2014	MHW	6	16,8
31	5 - 10 Oct 2015	WE	6	16,55
32	7 - 10 Nov 2015	WE	3	19.05
33	22 - 28 May 2018	MHW	7	18,4
34	08 - 13 Jun 2018	WE	6	17,3
35	05 - 14 Jan 2020	MHW	10	21,1

Table 4.1. continued.

Table 4.1 shows the total number of MHWs and WEs that were calculated as well as the events dates, type of warm water event, how many days the event lasted and the maximum SST per event. From January 2003 to March 2020, just over 17 years, 35 MHWs and WEs were identified (Table 4.1). Of the 35 events, 14 are MHWs and 21 are WEs (Table 4.1). In order to see the distribution of the number of MHW and WE days and maximum temperature, they will be described with the use of histograms in Figure 4.3 and Figure 4.4.

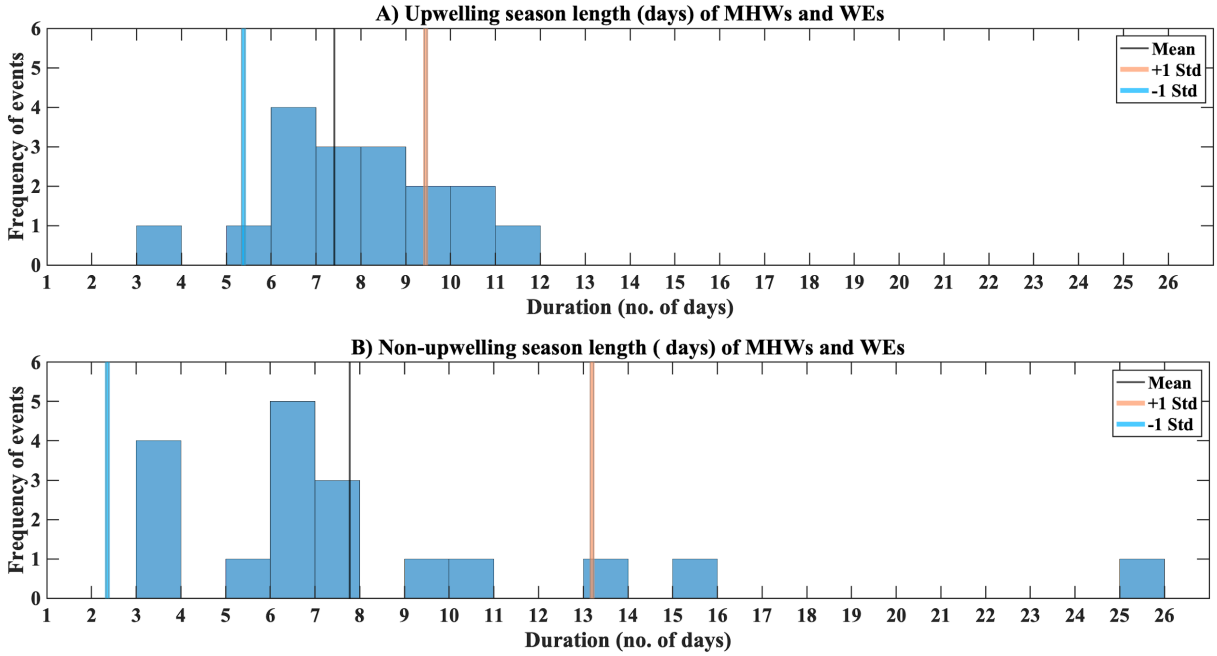

Figure 4.3: Bar graph indicating the frequency of the duration (number of days) of MHW and WE events in the CSIR SST Cape Point time series from 2003 to March 2020 in the A) upwelling season and B) non-upwelling season. The mean number of total days (black), +1 standard deviation (orange) and -1 standard deviation (light blue) are also indicated for each season.

Figure 4.3 depicts the number of days of each of the MHWs and WEs in Table 1 in the CSIR Cape Point station dataset. In the upwelling season (Figure 4.3 A), the mean number of days is 7.4 days. While the non-upwelling season has a slightly higher mean number of days of 7.78 days (Figure 4.3 B) both seasons have a mean number of MHWs and WEs total days between 7 and 8 days. Both seasons have the same mean number of days but their distribution is quite different. In the upwelling season the range between 1 standard deviation is between 5 to 10 days, while in the non-upwelling season has a much larger range between 2 to 14 days. In the upwelling season the distribution of the number of events is closer to the mean, with only one event lasting between 3 to 4 days and the longest event lasting being between 11 to 12 days (Figure 4.3 A). In the non-upwelling season, the lowest number of days is in the 3 to 4 days category and 4 events occur between 2003 and March 2020. The highest number of days in the non-upwelling season is between 25 to 26 days (Figure, 4.3 B), recorded as event number 15 in Table 1 and therefore no event exceeds a one month duration at the mooring location.

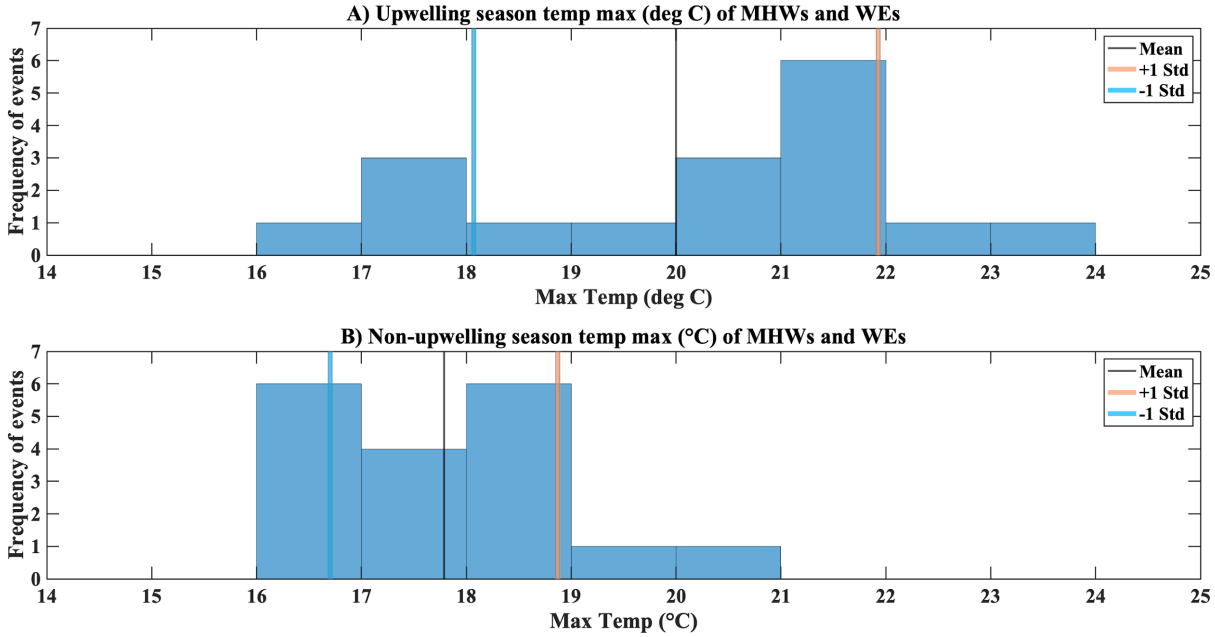

Figure 4.4: Bar graph indicating the frequency of the maximum temperature (°C) of MHWs and WEs in the CSIR SST Cape Point time series from 2003 to March 2020 in the A) upwelling season and B) non-upwelling season. The mean maximum temperature (black), +1 standard deviation (orange) and -1 standard deviation (light blue) are also indicated for each season.

Figure 4.4 depicts the maximum SST of the MHWs and WEs in Table 1 in the CSIR Cape Point mooring dataset. In contrast to the mean number of days per event (Figure 4.3), the mean maximum SST between the upwelling and the non-upwelling season is quite different. In the upwelling season the mean maximum SST value is 20°C (Figure 4.4 A). While, in the non-upwelling season the mean maximum SST is more than 2°C lower at 17.79°C (Figure 4.4 B). The distribution of the maximum SST value is much smaller in the non-upwelling season with 1 standard deviation between 16°C to 19°C than the upwelling season between 18°C to 22°C. The event with the lowest maximum SST in the CSIR is the same for upwelling and non-upwelling season, between 16°C and 17°C (Figure 4.4). The highest maximum SST in the non-upwelling season has a SST value between 19°C and 20°C (Figure 4.4 B). In the upwelling, the highest maximum is a few degrees higher with a SST value between 23°C and 24°C (Figure 4.4 A), recorded as event number 27 in Table 1. MHW number 27 is a WE from the 8th to the 13th of February 2014 (Table 1).

4.3 SST *in situ* and satellite dataset comparison

In this subsection the climatologies and number of MHWs and WEs in the half-hourly CSIR, daily CSIR, CCI and REMSS from 2003 to 2020 will be compared.

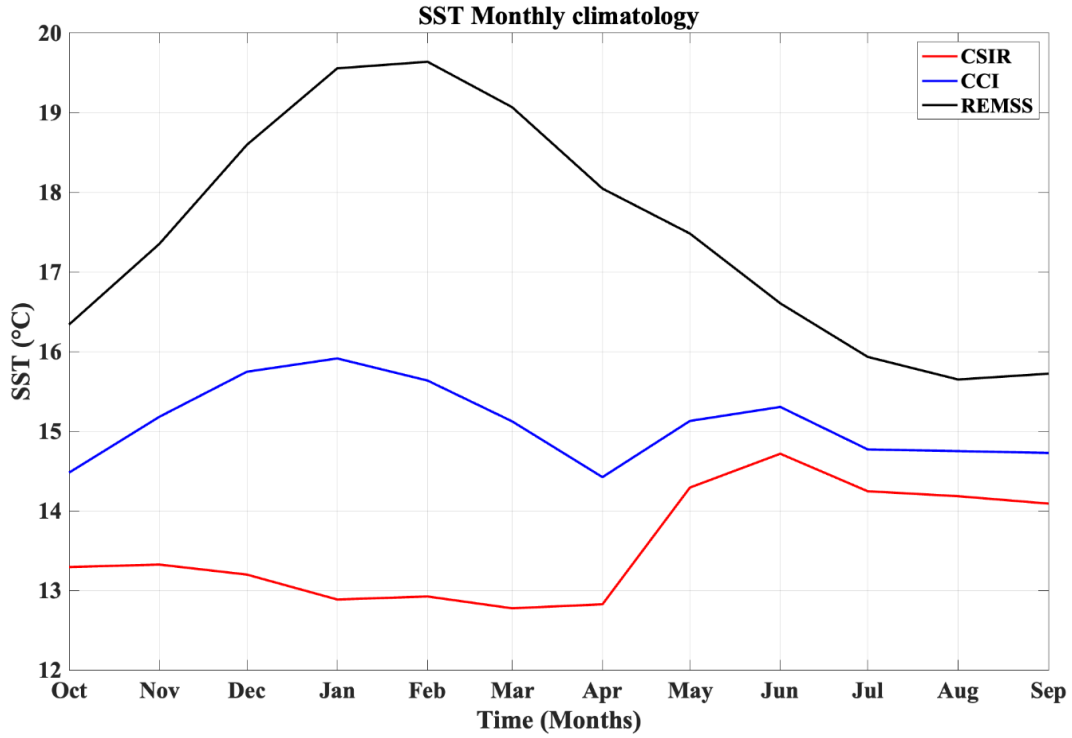

Figure 4.5: Monthly climatological time series of half-hourly CSIR SST (°C) Cape Point SST (red), CCI SST (dark blue) and REMSS SST (black) between 2003 – 2020 from October to September.

Figure 4.5 shows the monthly climatology of SST for CSIR, CCI and REMSS time series. The CCI monthly climatology is the closest to the CSIR climatology (Figure 4.1). The CCI non-upwelling season has a similar pattern to the CSIR dataset. Both have the highest SST values in June and the lowest in April, although the CCI dataset has slightly higher values, between 0.5°C and 1.6°C, than the CSIR dataset (Figure 4.5). In the CSIR upwelling season the SST gradually decreases from 13.29°C in October to 12.79°C in March. The CCI upwelling season increases from 14.48°C in October to 15.91°C in January, 3.03°C above the CSIR climatology. The CCI dataset then decreases to 15.12°C in March, 2.3°C above the CSIR climatology.

The REMSS climatology has higher SST values compared to both CSIR and CCI climatologies. REMSS and CCI have a similar pattern of overestimating the SST in the upwelling season and also have higher SST in summer than in winter, which is a concern

(Figure 4.5). The REMMS climatology starts in October 3.05°C above CSIR climatology. The REMSS SST increases until February, 6.71°C above CSIR dataset (Figure 4.5). Throughout the rest of the REMSS upwelling season the SST decreases to 6.2°C above CSIR dataset in March. REMSS non-upwelling season only has a similar pattern at the CSIR and CCI climatologies at the end of the non-upwelling season, the REMSS SST decreases at the start of the non-upwelling season with SST 1.46°C above CSIR dataset, while the CSIR and CCI climatologies increase (Figure 4.5).

Figure 4.6 shows the number of MHWs and WEs identified in the half-hourly CSIR, daily CSIR, CCI and REMSS SST time series. In the half-hourly CSIR (Figure 4.6 A & B, Table 1) there are a total of 35 events. Of those 35 events, 17 occurs in the upwelling season (Figure 4.6 A) and 18 occurs in the non-upwelling season (Figure 4.6 B). The highest number of MHW and WE events in the upwelling season are five events in 2003, with the lowest being 0 events in 2007, 2009, 2017 and 2018. The non-upwelling season has no MHWs or WEs in 2003, 2006, 2010, 2011, 2013, 2015, 2016, 2017 and 2019. The highest number of events in the non-upwelling season occurred in 2007 with 5 events.

Averaging the half-hourly to make a CSIR daily time series, to help compare MWH and WE calculation using the satellite datasets, leads to 75 events identified (Figure 4.6 C & D), more than double the half-hourly CSIR total events. The daily CSIR has 31 MHWs and 45 WEs. The daily CSIR has a total of 41 events in the upwelling season (Figure 4.6 C) and a total of 34 events in the non-upwelling season (Figure 4.6 D). The upwelling season and non-upwelling season has a correlation coefficient of -0.1538 and a P-value of 0.5424. The highest number of events in the CSIR daily occurs in the 2007 non-upwelling season with 9 MHW and/or WE events (Figure 4.6 D), while the half hourly CSIR has 5 events during this period.

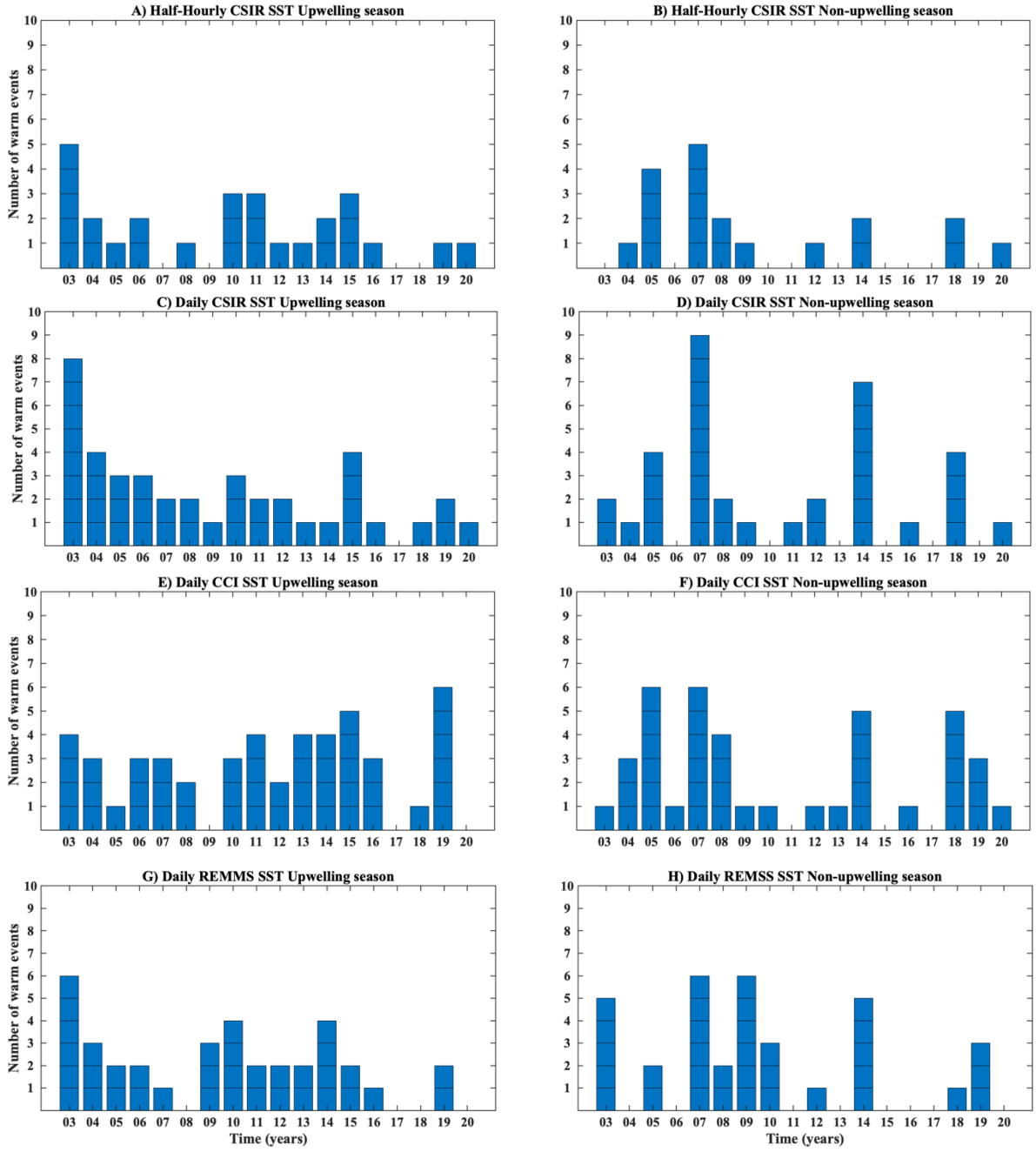

Figure 4.6: Bar graphs indicating the number of MHWs and WEs between 2003 and 2002 in the upwelling season for A) half-hourly CSIR SST, C) daily CSIR SST, E) daily CCI SST and G) daily REMSS SST and for non-upwelling season B) half-hourly CSIR SST, D) daily CSIR SST, F) daily CCI SST and H) REMSS SST.

In the CCI time series there are 88 MHWs and WEs events (Figure 4.6 E & F), similar to the CSIR daily dataset, double the number CSIR half-hourly events. The daily CCI has 38 MHWs and 50 WEs. The CCI dataset has 48 events extreme warm water events in the upwelling season (Figure 4.6 E) , and a total of 40 events in the non-upwelling season (Figure 4.15 F). The highest number of events in the CCI dataset is 6 events, occurring in the 2019 upwelling season

and 2005 and 2007 non-upwelling seasons (Figure 4.6 E & F). The half-hourly CSIR dataset has less MHW and WEs events during these periods with 1, 3 and 5 events (Figure 4.6 A & B).

In the REMSS time series there are 70 MHWs and WEs events (Figure 4.6 G & H), similar to the CSIR daily and CCI datasets, double the number CSIR half-hourly events. The daily REMSS has 27 MHWs and 43 WEs. The REMSS dataset has a total of 36 events in the upwelling season (Figure 4.6 G) and a total of 34 events in the non-upwelling season (Figure 4.6 H). The highest number of events in the REMSS dataset is 6 events, occurring in 2003 upwelling season and 2007 and 2009 non-upwelling season (Figure 4.6 G & H). The half-hourly CSIR dataset has fewer MHW events during these periods with 5, 5 and 1 events (Figure 4.6 A & B).

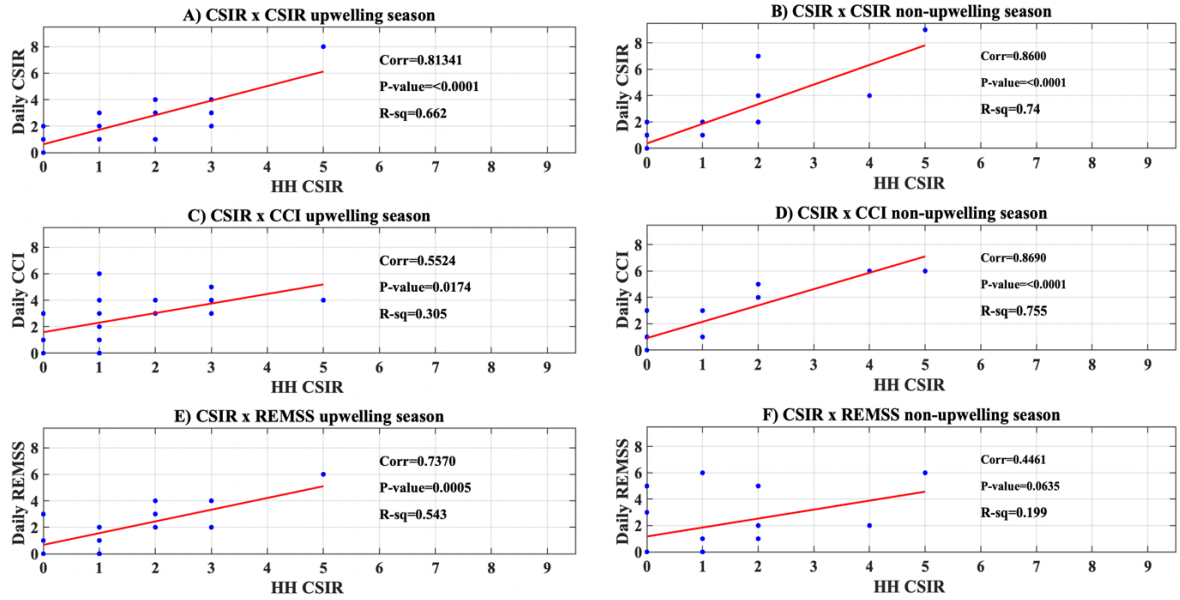

Figure 4.7: Plotted are the scatter plots, with the line of best fit, to compare the number of events occurring in the upwelling season between A) half-hourly CSIR and daily CSIR, C) half-hourly CSIR and daily CCI and E) half-hourly CSIR and daily REMSS. Also plotted is the number of events occurring in the non-upwelling season B) half-hourly CSIR and daily CSIR, D) half-hourly CSIR and daily CCI and F) half-hourly CSIR and daily REMSS. The correlation value, P-value and the R-squared for each comparison is also indicated.

Figure 4.7 shows the comparison of the number of events identified in the half-hourly CSIR dataset with the daily CSIR, CCI and REMSS visual with a scatter plot and a line of best fit as

well as quantitatively with the correlation, p-value and the R-squared. In the upwelling season, the daily CSIR has the highest significant correlation of 0.81 and also with the lowest scatter, 0.66 (Figure 4.7 A). The second best significant correlation is with REMSS, 0.73, and also has a lower R-squared value, 0.54, therefore more scatter than the CSIR daily comparison (Figure 4.7 B). CCI has the lowest significant correlation of 0.55 and also has the highest scatter with a R-squared value of 0.30 (Figure 4.7 A).

In the non-upwelling season, the daily CCI has the highest significant correlation of 0.87 also the highest R-squared, 0.76, so the half-hourly CSIR and the CCI also have the lowest scatter (Figure 4.7 A). The second highest significant correlation is 0.86 with the daily CSIR and has more scatter with a R-squared value of 0.74. REMSS has a correlation of 0.44 and has the highest scatter with a R-squared value 0.99

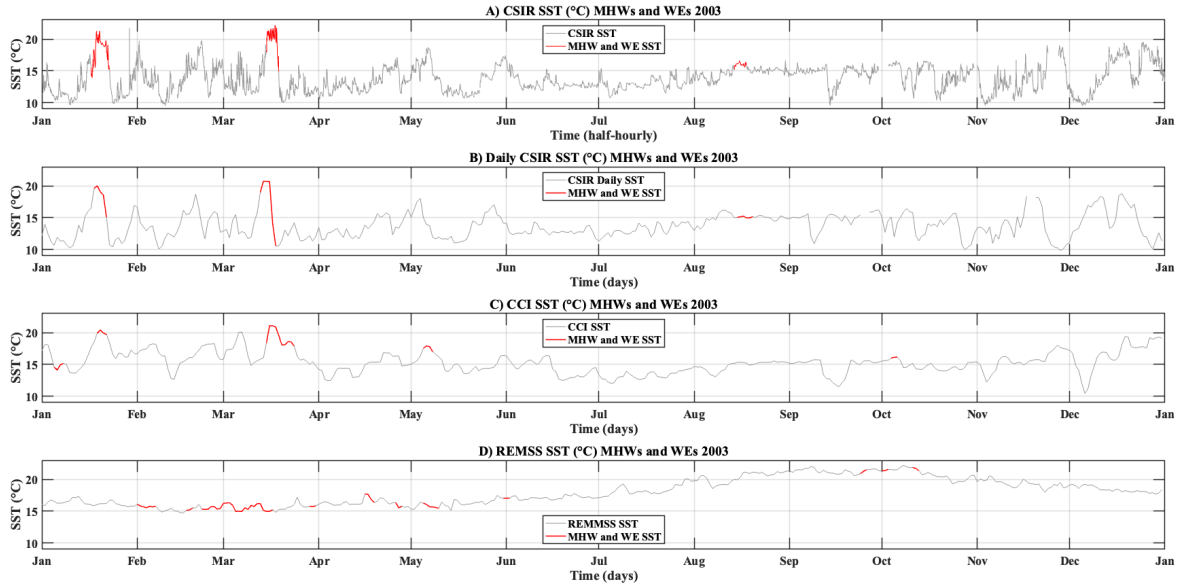

Figure 4.8: A) CSIR half-hourly, B) daily CSIR, C) daily CCI and D) daily REMMS (grey) SST (°C) for 2003 at the CSIR Cape Point mooring station with the identified MHWs and WEs (red) for each dataset.

Figure 4.8 shows the time series of the CSIR half-hourly, daily CSIR, daily CCI and daily REMSS and the MHWs and WEs identified in the year 2003. In the CSIR time series two MHWs events, from the 15th to the 22nd of January and the 13th to the 18th of March, and one WEs, from the 14th to the 18th of August (Table 1; Figure 4.7 A). As the daily CSIR is an average of the half-hourly CSIR, the events which occur in the half-hourly CSIR also are observed in the daily CSIR with a couple days difference in the event start and end dates. The

MHW occurs in January in the CCI time series as well but from the 19th to the 22nd of January (Figure 4.7 B). The closest event in the REMSS time series to the January event, is in a WE event in February from the 17th to the 20th (Figure 4.7 C). The CCI also has a MHW near the CSIR event which occurs in March, from 15th to the 24th of March (Figure 4.7 B). The REMSS has an event during the CSIR March event but starts in February, the event lasts from the 22nd to the 17th of March Figure 4.7 C). Both CSIR and REMSS do not identify the CSIR WE in August (Figure 4.7 B & C). The CCI time series has a total of 5 events in 2003 and therefore has two more than the CSIR but three of the events were in different periods to the CSIR events (Figure 4.7 B). The REMSS has a total of 11 events, two of which are over the same period as the CSIR and 9 events in different periods (Figure 4.7 C).

4.4 The influence of wind on CSIR MHW formation and dissipation

In this subsection, the wind direction on the day of the onset and end of each of the CSIR MHW and WE events will be recorded. Then every combination of wind direction at the start and end of a MHW or We event will be examined through an example event. Each example of the wind combinations will be analysed with ERA5 V and U wind and CCI anomaly maps (the REMSS anomaly plots for the example can be in Chapter 8, CCI was used as the climatology is more similar to the CSIR than REMSS).

			Upwelling season		Non-upwelling season	
No.	Event dates	Event Type	Wind direction at event start	Wind direction at event end	Wind direction at event start	Wind direction at event end
1	15 - 22 Jan 2003	MHW	NW	SE	-	-
2	13 - 18 March 2003	MHW	NW	SE	-	-
3	14 - 18 Aug 2003	WE	-	-	NW	NW
4	18 - 26 April 2004	MHW	-	-	NW	SE

Table 4.2: A table describing the wind direction at the onset and dissipation of the MHW or WE events seen in Table 1, separated into upwelling and non-upwelling seasons at the CSIR Cape point mooring from January2003 to March 2020. The wind direction is recorded by where the wind is coming from, southerly (S), northerly (N), easterly (E) and westerly (W).

			Upwelling season		Non-upwelling season	
No.	Event dates	Event Type	Wind direction at event start	Wind direction at event end	Wind direction at event start	Wind direction at event end
5	27 Jan - 04 Feb 2005	WE	NW	SE	-	-
6	20 - 27 April 2005	MHW	-	-	NW	SE
7	9 - 12 May 2005	WE	-	-	NW	SE
8	16 - 25 May 2005	WE	-	-	NW	SE
9	10 - 16 Mar 2006	MHW	SE	SE	-	-
10	25 Dec - 01 Jan 2006	WE	NW	SE	-	-
11	13 - 18 Apr 2007	MHW	-	-	SE	SE
12	24 Apr - 04 May 2007	MHW	-	-	NW	SE
13	24 Jul - 06 Aug 2007	MHW	-	-	SW	NW
14	11 - 17 Aug 2007	WE	-	-	NW	SE
15	01 - 24 Sep 2007	MHW	-	-	NW	SE
16	25 - 30 May 2008	WE	-	-	NW	NW
17	30 Jul - 03 Aug 2007	MHW	-	-	NW	SE
18	04-08 June 2009	WE	-	-	NW	SE
19	07 - 13 Feb 2010	WE	NW	SE	-	-
20	24 - 30 Mar 2010	WE	NW	SE	-	-
21	20 - 25 Oct 2010	WE	NW	SE	-	-
22	01 - 04 Apr 2011	WE	-	-	NW	SE
23	25 Oct - 01 Nov 2011	MHW	NW	SE	-	-
24	07 - 15 Nov 2011	WE	NW	SE	-	-
25	01 - 05 Mar 2012	WE	SE	SE	-	-
26	30 Sep - 06 Oct 2012	WE	-	-	NW	SW
27	08 Feb - 13 Feb 2014	WE	NW	SE	-	-
28	25 Mar - 04 Apr 2014	MHW	NW	SE	-	-

Table 4.2. continued.

			Upwelling season		Non-upwelling season	
No.	Event dates	Event Type	Wind direction at event start	Wind direction at event end	Wind direction at event start	Wind direction at event end
29	09 - 12 May 2014	WE	NW	SE	-	-
30	25 - 30 June 2014	MHW	-	-	NW	SE
31	07 - 10 Oct 2015	WE	NW	NW	-	-
32	07 - 10 Nov 2015	WE	NW	SE	-	-
33	22 - 28 May 2018	MHW	-	-	NW	NW
34	08 - 13 Jun 2018	WE	-	-	NW	NW
35	05 - 14 Jan 2020	MHW	NW	SE	-	-

Table 4.2. continued.

Table 4.2 is similar to Table 4.1 as it records the dates and type of warm water event, but it also has a record of the wind direction at the start and at the end of the MHWs or WEs. Of the 17 events (Figure 4.6) in the upwelling season, 14 events start with north-westerly and end with south-easterly wind. Two of the upwelling season events starts and ends with south-easterly winds and 1 event starts and ends with both north-westerly winds (event 31, Table 4.2). Of the 18 events (Figure 4.6) in the non-upwelling season, 11 of the events starts with north-westerly wind and ends with south-easterly wind. Only 1 event in the non-upwelling season starts and ends with south-easterly winds (event 11) and 4 events start and end with north-westerly wind. Two wind combinations which are not seen in the upwelling season is 1 event starting with south-westerly winds and ending with north-westerly winds (event 13) and 1 event starting with north-westerly winds and ending with south-westerly winds (event 25, Table 4.2).

4.4 A. North-westerly formation and south-easterly dissipation of MHWs or WEs

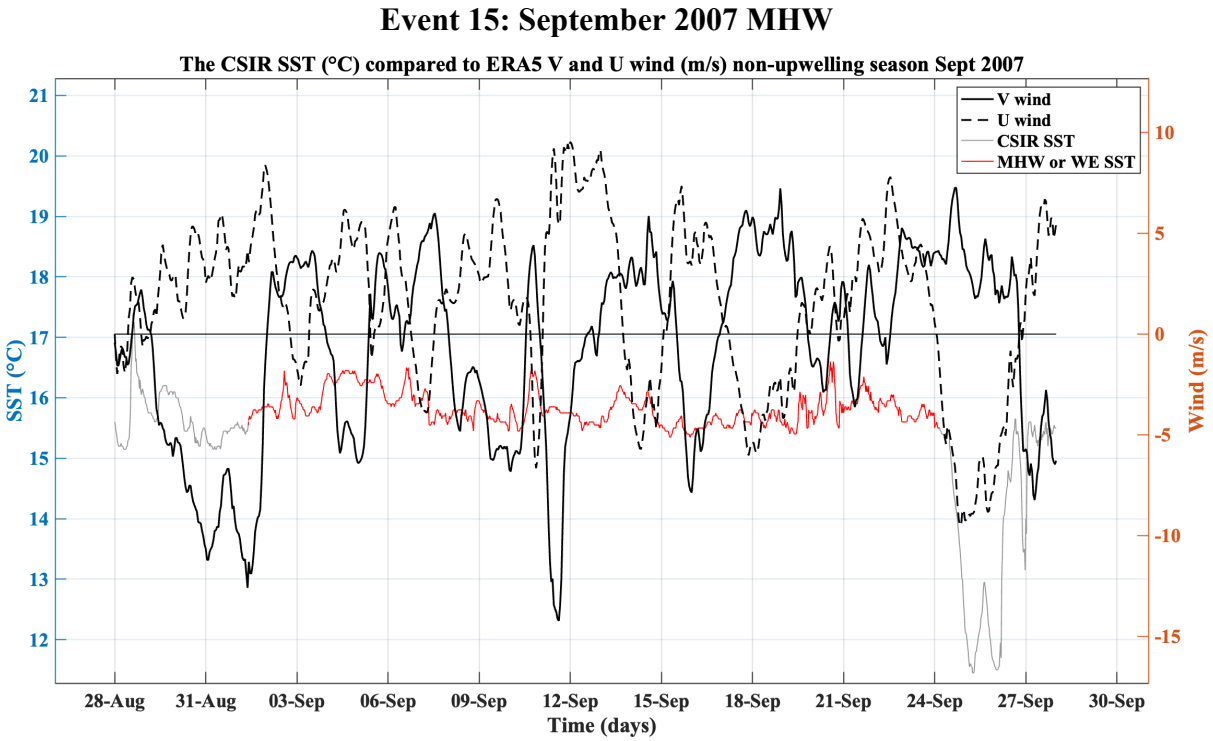

Figure 4.9: CSIR SST (°C) and ERA5 wind (m s^{-1}) are plotted in the non-upwelling season 2007 over Event 15 (01 – 24 September Table 2), at Cape Point CSIR station in the SBUS. Plotted is the original CSIR SST time series (grey), defined MHWs or WEs SST (red), V wind component (black) and U wind component (dashed black).

In Figure 4.9 the CSIR SST and the ERA5 wind for the September 2007 MHW is plotted (Table 1 & 2). As seen in Table 1, the MHW between the 1st and the 25th of September is the longest event which occurred in the 17-years from 2003 to March 2020. The SST increases from 15.15°C on the 31st of August to 15.55°C starting the MHW. Before and as well as at the onset of the MHW event, the wind is north-westerly (Figure 4.9; Table 2). At the onset of the MHW on the 1st of September the V wind is -12.6 m s^{-1} and the U wind is 5.3 m s^{-1}. During the MHW event the SST varies between 15.45°C and 16.6°C (Figure 4.9). The event has 9 short periods where the SST goes below the 90th percentile for a couple hours, but the SST does not decrease below 15.36°C (Figure 4.9). During the MHW the wind direction shifts every day or two, predominantly between south-easterly and north-westerly. From the 21st of September the SST slowly begins to decrease from 16.3°C. Until the end of the event on the 24th of September, when the SST rapidly decreases from 15.55 to 11.45°C on the 25th of September. On the 24th

of September the wind is south-easterly and increases from 3.5 m s^{-1} to 7.2 m s^{-1} V wind and decreases from -0.2 m s^{-1} to -9.5 m s^{-1} throughout the day, leading to the end of the MHW.

Figure 4.10 shows the spatial progression of the September 2007 MHW (Figure 4.9; Table 1 & 2) through CCI SST anomaly plots. On the day before the MHW, on the 31st of August there is a water mass with SSTAs between 1°C and 2°C, with the start of a MHW, to the north and the west of the CSIR mooring (Figure 4.10 A). On the day of the MHW, the 1st of September, the region of high SSTAs increases to SSTAs between 1°C and 2°C and the area of the MHW has increased and is just north of the CSIR mooring (Figure 4.21 B). The water mass with SSTAs between 1°C and 2°C has also moved over the CSIR station. Throughout the MHW the event thins and moves further northwest and decreases in SSTA values and MHW area over time (Figure 4.10 C & B). The day the MHW ends, the 24th of September, the area of the MHW has dissipated further with a small MHW area at about -33°S and 17.8°E. There is also no longer SSTAs between 1°C and 2°C over the CSIR mooring (Figure 4.10 E). The day after the event the region of positive SSTAs remains the same as the day before (Figure 4.10 F). In the REMSS dataset there is a MHW throughout the Cape Peninsula Cell on the day before the MHW and persists throughout and after the end of the September 2007 MHW (Figure 8.1).

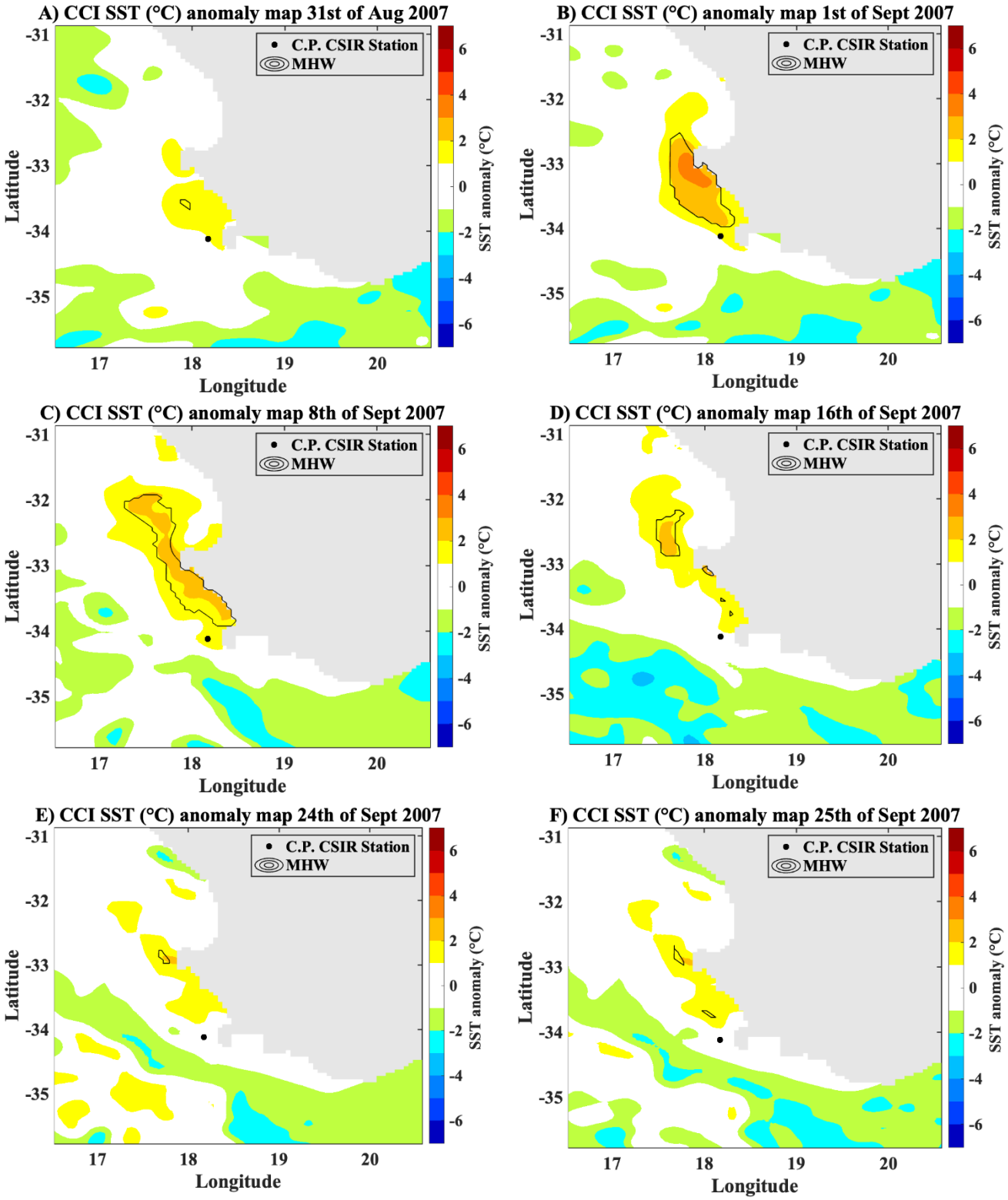

Figure 4.10: September 2007 MHW event CCI SST (°C) anomaly plots with MHW outline for A) the 31st of August (1 day before MHW begins), B) the 1st of September (day MHW begins), C) the 8th of September (7 days after the start of the MHW), D) 16th of September (15 days after the start of the MHW), E) the 24th of September (day the MHW ends) and F) the 25th of September (1 day after MHW ends).

4.4 B. South-easterly formation and south-easterly dissipation of MHWs or WEs

Event 9: March 2006 MHW

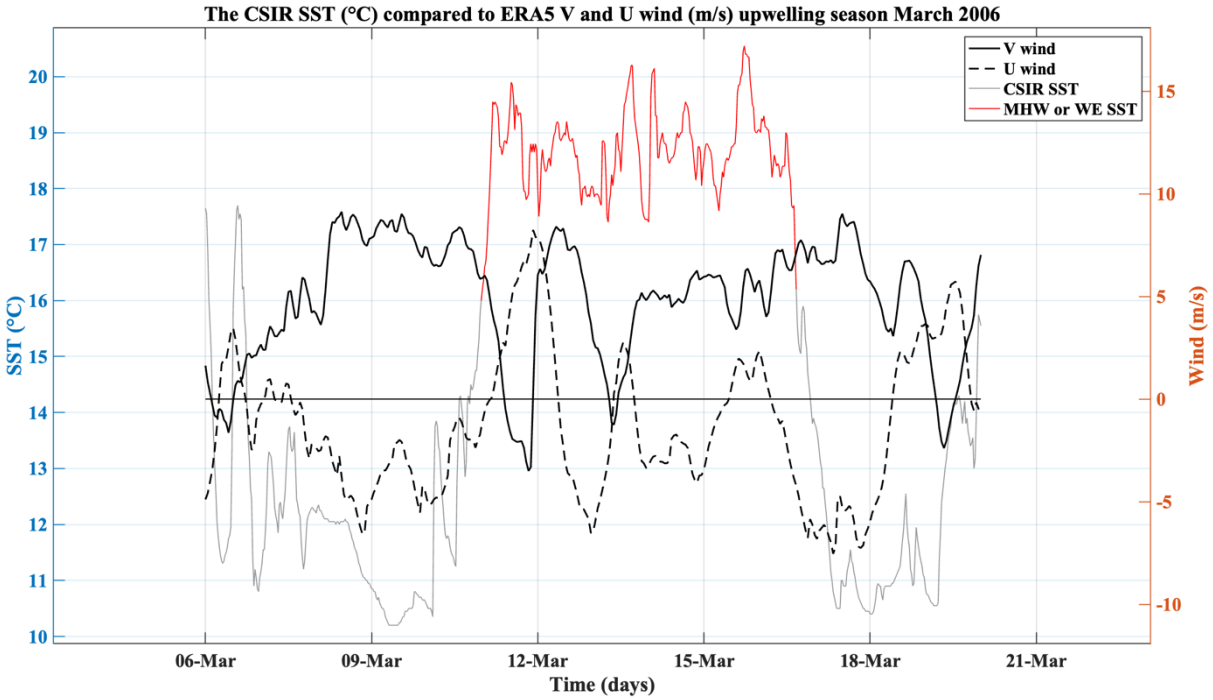

Figure 4. 11: CSIR SST (°C) and ERA5 wind (m s^{-1}) are plotted in the upwelling season 2006 over Event 9 (10 – 16 March, Table 2), at Cape Point CSIR station in the SBUS. Plotted is the original CSIR SST time series (grey), defined MHWs or WEs SST (red), V wind component (black) and U wind component (dashed black).

In Figure 4.11 the CSIR SST and the ERA5 wind for the March 2006 MHW is plotted (Table 1 & 2). As seen in Table 2, the event 9 MHW between the 10th to the 16th of September. On the 10th the SST increases from 10.36°C, onsetting the MHW at 16°C, to 19.55°C on the 11th of March (Figure 4.11). For over four days before the onset of the MHW the winds are south-easterly. At the onset of the MHW the V wind is 6.6 m s^{-1} and the U wind is -2 m s^{-1}. Over the MHW period the SST ranges between 16°C to 20.55°C. The wind shifts to a north-westerly at the start of the event for less than a day then shifts south-westerly before turning south-easterly for almost the rest of the event. The SST begins to slowly decrease from the 15th at 20.55°C. On the 16th the SST decreases from 18.95°C, past 16.2°C ending the MHW, to 10.6°C at the start of the 17th of March. Throughout the 16th of March the wind is south-easterly, at the end of MHW the V wind is 7.3 m s^{-1} and the U wind is -4.3 m s^{-1}.

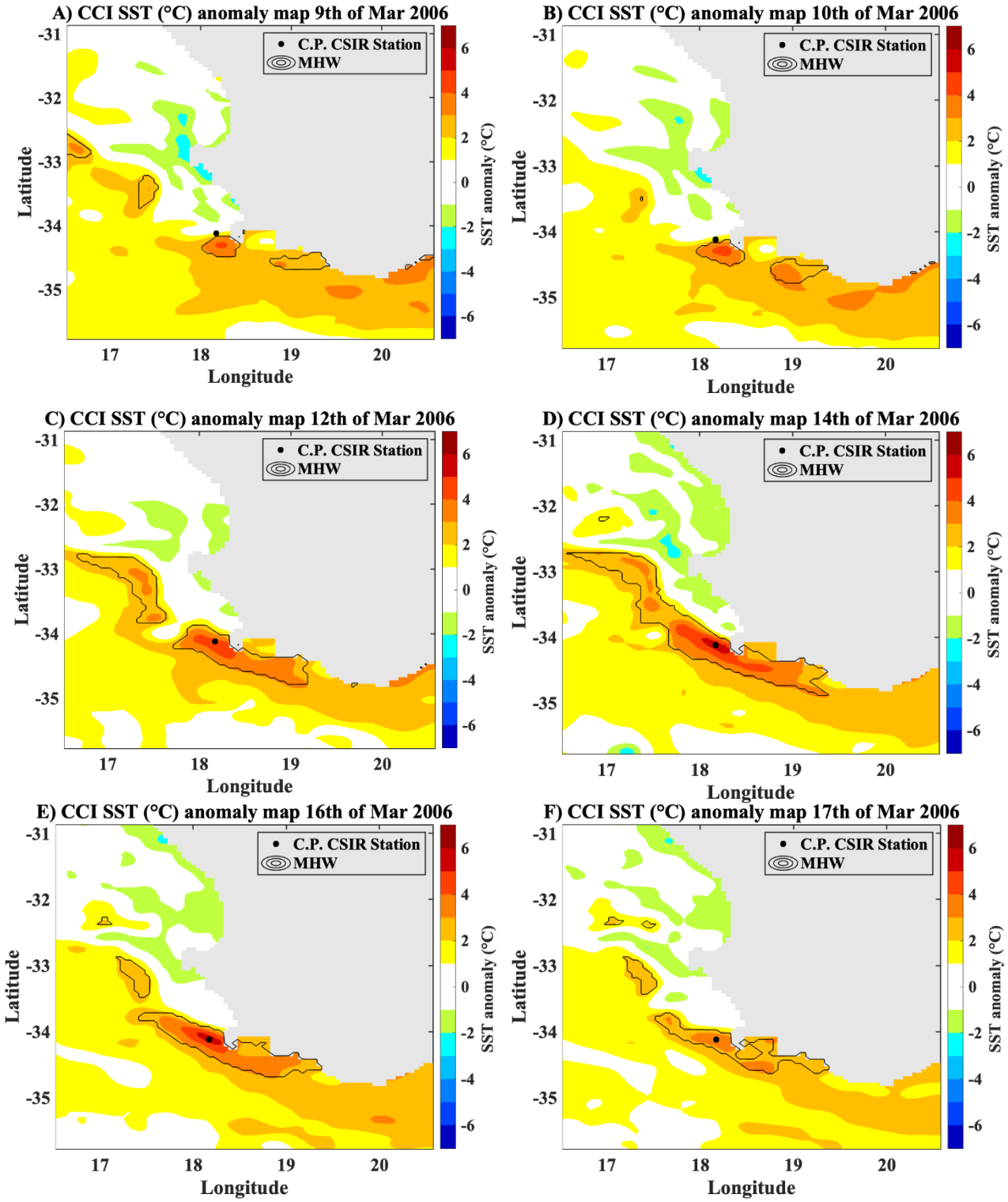

Figure 4.12: March 2006 MHW event CCI SST (°C) anomaly plots with MHW outline for A) the 9th of March (1 day before MHW begins), B) the 10th of March (day MHW begins), C) the 12th of March (2 days after the start of the MHW), D) 14th of March (4 days after the start of the MHW), E) the 16th of March (day the MHW ends) and F) the 17th of March (1 day after MHW ends).

Figure 4.12 shows the spatial progression of the March 2006 MHW (Figure 4.11; Table 1 & 2) through CCI SST anomaly plots. On the day before the MHW, on the 9th of March to the south of the CSIR there are positive SSTAs and a MHW from off Cape point to further offshore from the CSIR mooring (Figure 4.12 A). Above the mooring there are negative SSTAs values (Figure 4.12 A). The day the CSIR MHW starts, on the 10th of March, the MHW has increased spatially further offshore and SSTAs between 1°C and 2°C have moved over the CSIR mooring (Figure 4.23 B). During the CSIR MHW the MHW has moved northward, over the CSIR mooring and further south-eastward. The SSTAs between 1°C and 2°C to the north-west of the CSIR mooring also have developed to a MHW (Figure 4.12 C). On the 14th of March the two MHWs can be seen to have connected to form one MHW (Figure 4.12 D). On the day the CSIR MHW ends, on the 16th of March, the MHW SSTAs have decreased but the CCI dataset still shows the MHW over the CSIR mooring location with SSTAs between 5°C and 6°C (Figure 4.12 E). The day after the CSIR MHW ends, the CCI MHW has decreased in area but is still over the CSIR mooring but the SSTAs have decreased to between 3°C and 4°C (Figure 4.12 F). There is no MHW in the REMSS SST dataset during the period of the March 2006 MHW (Figure 8.2).

4.4 C. North-westerly formation and south-westerly dissipation of MHWs or WEs

Event 26: September/October 2012 WE

In Figure 4.13 the CSIR SST and the ERA5 wind for the September/ October 2012 WE is plotted (Table 1 & 2). As seen in Table 2, the September/October 12 WE between the 30th of September to the 6th of October. The SST increases from 15.15°C to more than 15.7°C, starting the WE. During the onset of the WE the wind is north-westerly, -6.55 m s^{-1} V wind and 2.67 m s^{-1} U wind. The SST increases to 16.8°C and then decreases to 15.3°C, with a small increase on the 5th of October to 16.3°C. During the WE the wind shifts to south-easterly wind for a day on the 1st of October. The wind is mostly north-westerly until the 4th of October, then the wind is south-westerly until the 7th of October. The WE ends on the 6th of October having gradually decreased below 15.45°C and below the 90th percentile.

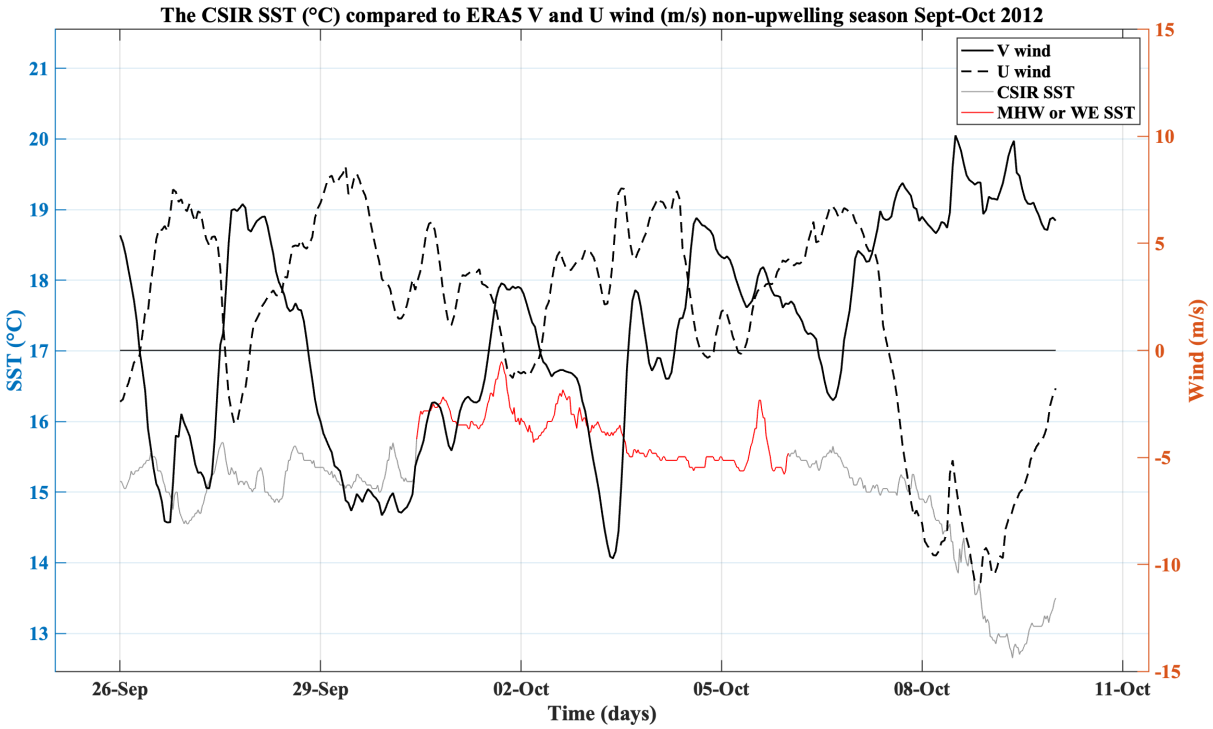

Figure 4.13: CSIR SST (°C) and ERA5 wind (m s-1) are plotted in the non-upwelling season 2012 over Event 26 (30 September- 6 October, Table 2), at Cape Point CSIR station in the SBUS. Plotted is the original CSIR SST time series (grey), defined MHWs or WEs SST (red), V wind component (black) and U wind component (dashed black).

Figure 4.14 shows the spatial progression of the September/October 2012 WE (Figure 4.13; Table 1 & 2) through CCI SST anomaly plots. On the day before the CSIR WE, on the 29th of September, there is an area of SSTAs between 1°C and 2°C to the west of the CSIR mooring (Figure 4.14 A). The day of the CSIR WE, 30th of September, the SSTAs between 1°C and 2°C have extended further north and west. A CCI MHW has developed along the coast with SSTAs between 1°C and 3°C nearly over the CSIR mooring (Figure 4.14 B). During the CSIR WE, the CCI MHW extends further northward along the coast on the 2nd of October and has SSTAs between 1°C and 4°C (Figure 4.14 C). By the 4th of October the CCI MHW has almost dissipated but there are still SSTAs between 1°C and 2°C at the CSIR mooring (Figure 4.14 D). On the day the CSIR WE ends the CCI MHW has ended (Figure 4.14 E). The day after the CSIR WE ends the SSTAs decrease to between -1°C and 1°C (Figure 4.14 F). In the REMSS dataset there is a MHW throughout the Cape Peninsula Cell on the day before the WE and persists throughout and after the end of the September/October 2012 WE (Figure 8.3).

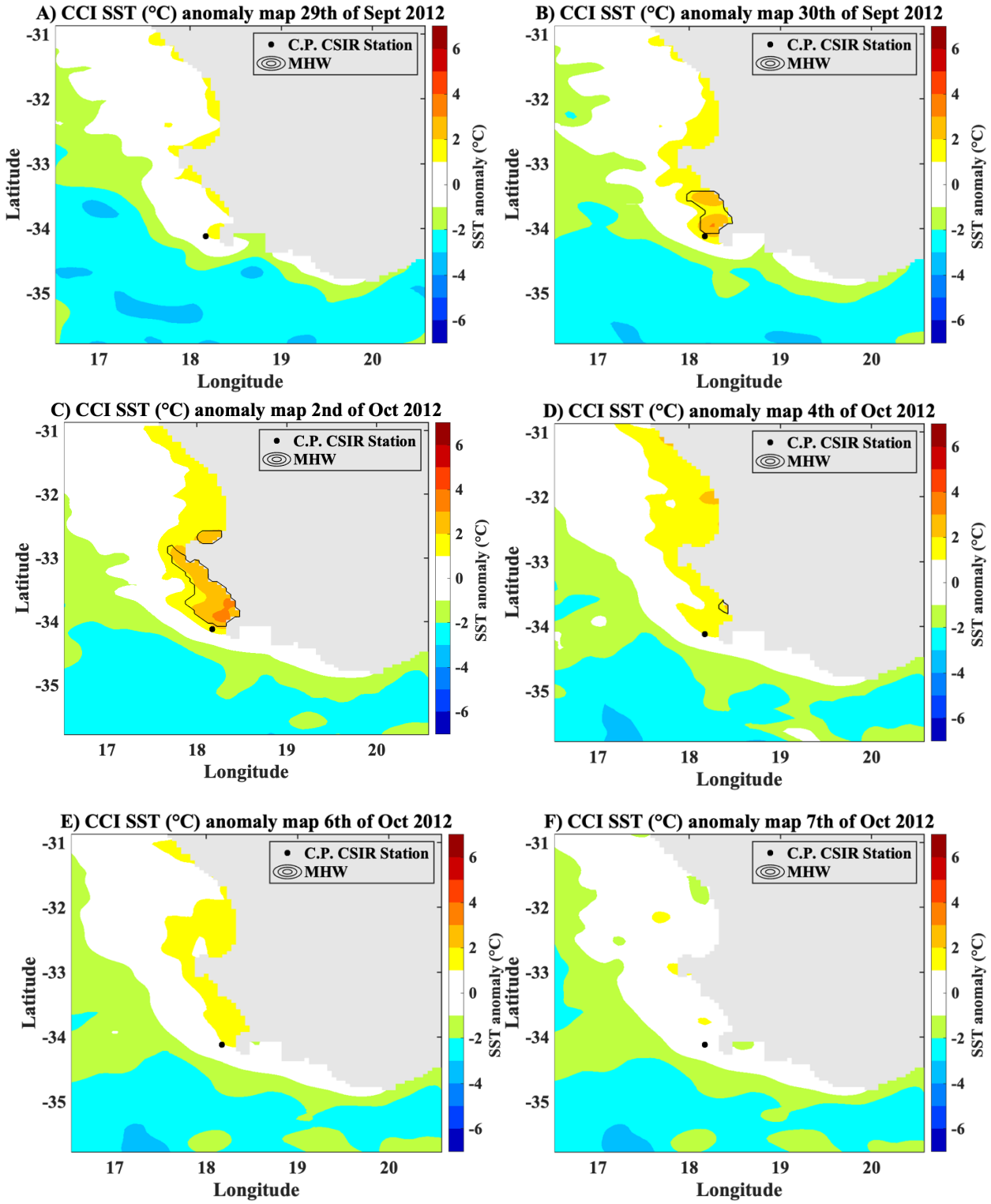

Figure 4.14: September/October 2012 WE event CCI SST (°C) anomaly plots with WE outline for A) the 29th of September (1 day before WE begins), B) the 30th of September (day WE begins), C) the 2th of October (2 days after the start of the WE), D) 4th of October (4 days after the start of the WE), E) the 6th of October (day the WE ends) and F) the 7th of October (1 day after WE ends).

4.4 D. North-westerly formation and north-westerly dissipation of MHWs or WEs

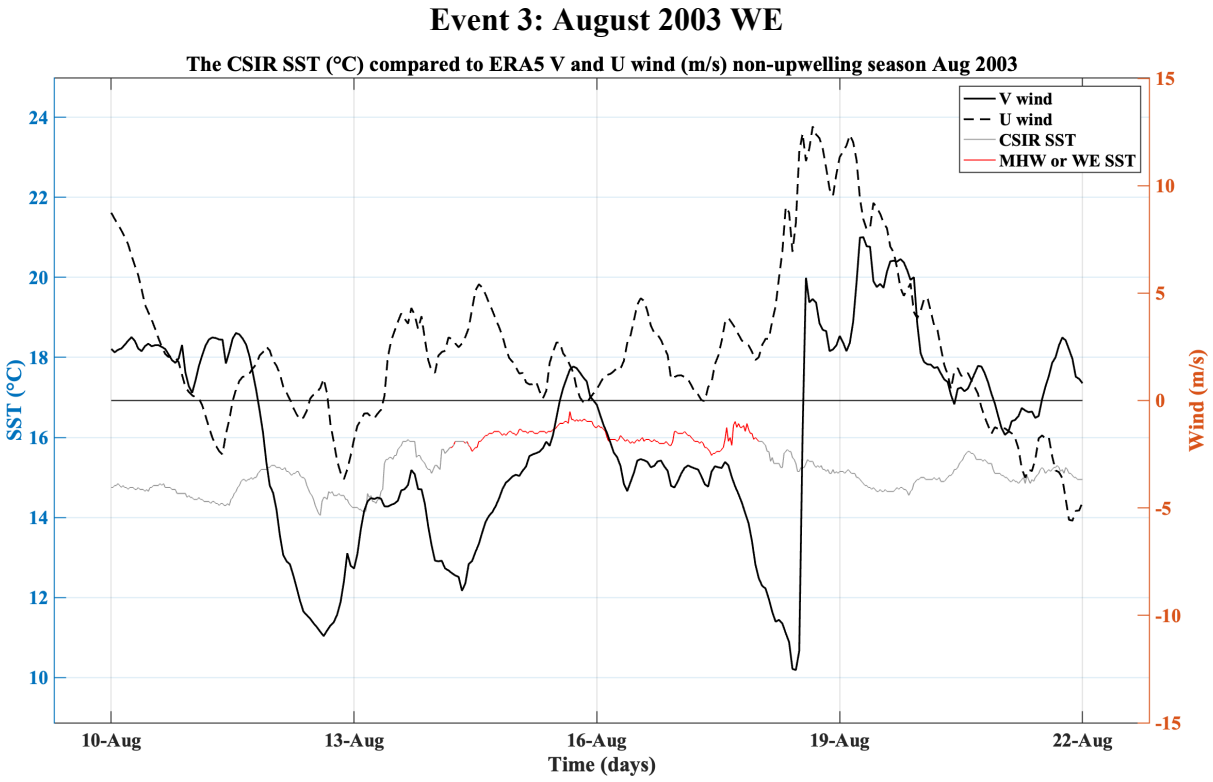

Figure 4. 15: CSIR SST (°C) and ERA5 wind (m s-1) are plotted in the non-upwelling season 2003 over Event 3 (14 – 18 August, Table 2), at Cape Point CSIR station in the SBUS. Plotted is the original CSIR SST time series (grey), defined MHWs or WEs SST (red), V wind component (black) and U wind component (dashed black).

In Figure 4.15 the CSIR SST and the ERA5 wind for the August 2003 WE is plotted (Table 1 & 2). As seen in Table 2, the event 3 WE between the 14th to the 18th of August. The onset of the WE occurs when the SST increases from 15.1°C on the 13th to 15.8, above the 90th percentile on the 14th of August. At the onset of the WE the wind is north-westerly, with the V wind being -7.6 m s^{-1} and the U wind being 2.9 m s^{-1}. The SST ranges between 15.75°C to 16.45°C for the WE. From the onset of the wind the wind shifts south-westerly on the 15th of August, then shifts back to north-westerly for the remainder of the WE. The WE ends when the SST decreases past 15.7°C on the 18th of August and decreases to 15.1°C throughout the day. The wind at the end of the WE is -8.5 m s^{-1} for the V wind and 1.8 m s^{-1} for the U wind.

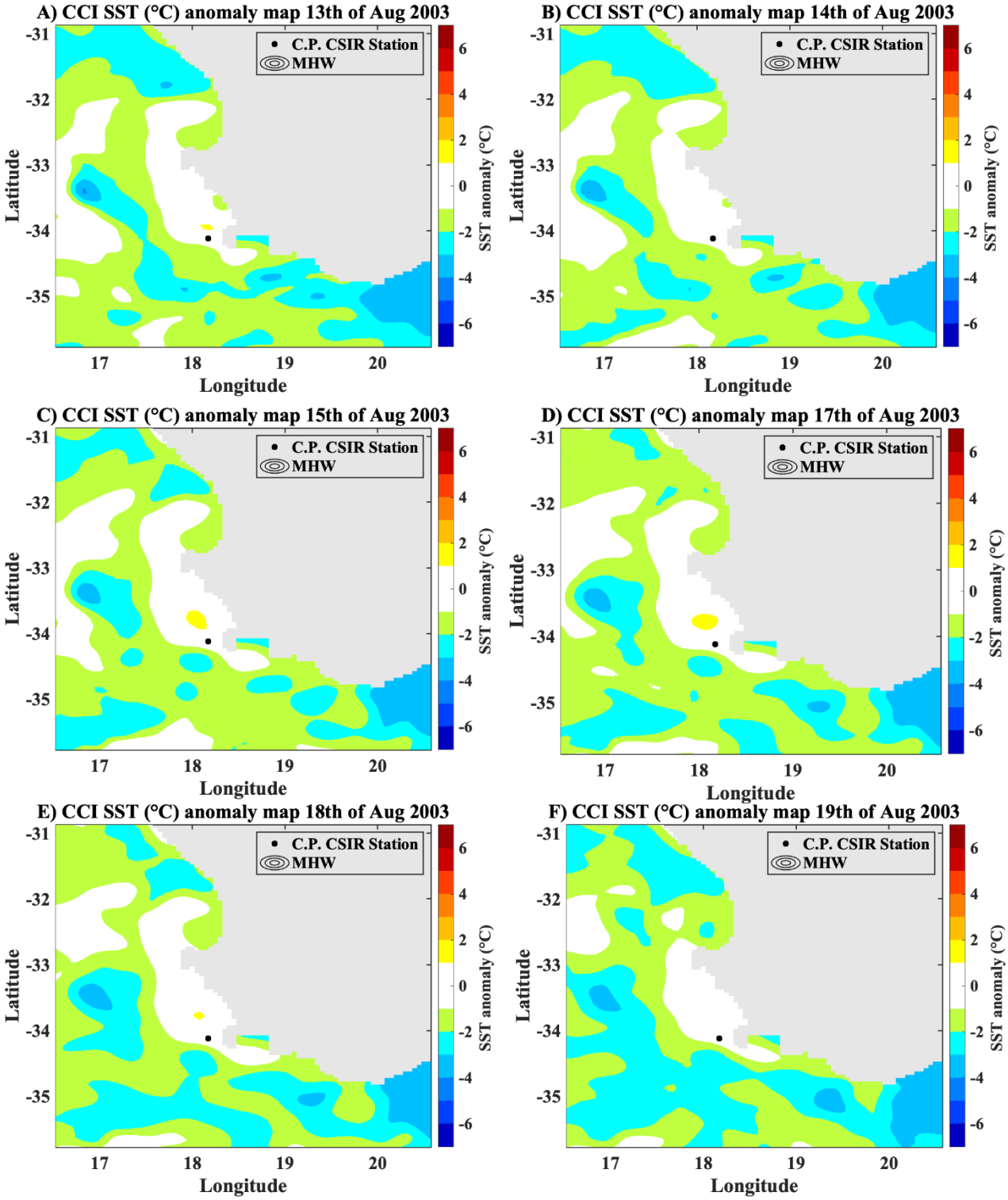

Figure 4.16: August 2003 WE event CCI SST (°C) anomaly plots with WE outline for A) the 13th of August (1 day before WE begins), B) the 14th of August (day WE begins), C) the 15th of August (1 day after the start of the WE), D) 17th of August (3 days after the start of the WE), E) the 18th of August (day the WE ends) and F) the 19th of August (1 day after WE ends).

Figure 4.16 shows the spatial progression of the July/August 2007 WE (Figure 4.15; Table 1 & 2) through CCI SST anomaly plots. For the period of the CSIR WE at the CSIR mooring the SSTAs are between -1°C and 1°C, further offshore the SSTAs values are with -3°C and -1°C. On the day before of the WE, on the 13th of August, there is a small area of SSTAs values between 1°C and 2°C slightly north of the CSIR mooring, which has dissipated the next day on the 14th of August (Figure 4.16 A & B). During the WE, on the 15th and the 17th of August, the small area of SSTAs values between 1°C and 2°C slightly north of the CSIR mooring is present again (Figure 4.16 C & D). The area of higher SSTA values can still be seen on the day the WE ends, the 18th of August, but has dissipated slightly (Figure 4.16 E). On the day after the WE, the 19th of August, there are no SSTAs values between 1°C and 2°C near the CSIR mooring. In the REMSS dataset, there is a MHW to the north of the CSIR mooring and along the west coast which extends southwards during the July/August 2007 WE and persists after the WE has ended (Figure 8.4).

4.4 E. South-westerly formation and north-westerly dissipation of MHWs or WEs

Event 13: July/August 2007 MHW

In Figure 4.17 the CSIR SST and the ERA5 wind for the August 2007 MHW is plotted (Table 1 & 2). As seen in Table 2, the event 13 MHW between the 24th July to the 6th of August. The MHW starts on the 24th of July when the SST increase from 15.4°C, past 15.7°C the 90th percentile, to 16.45°C. The wind at the start of the MHW is wind is south-westerly, with V wind of 2.3 m s^{-1} and u wind of 2.16 m s^{-1}. It is worth noting that just before the south westerly wind there was strong north-westerly wind with V wind values as low as -10.11 m s^{-1} and U wind as high as 9.4 m s^{-1}. During this period the SST has a range between 15.2°C on the 26th of July to 16.6°C on the 30th of July. The wind remains mostly westerly during the MHW, reaching U wind values of 13.3 m s^{-1}, except for just before the end of the event. The V wind shifts from northerly wind to southerly wind throughout the event. The event ends on the 6th of August when the SST decreases below 16.2°C. The wind during the end of the event is a strong north-westerly, with V wind value of -12.2 m s^{-1} and U wind with a value of 11.08 m s^{-1}.

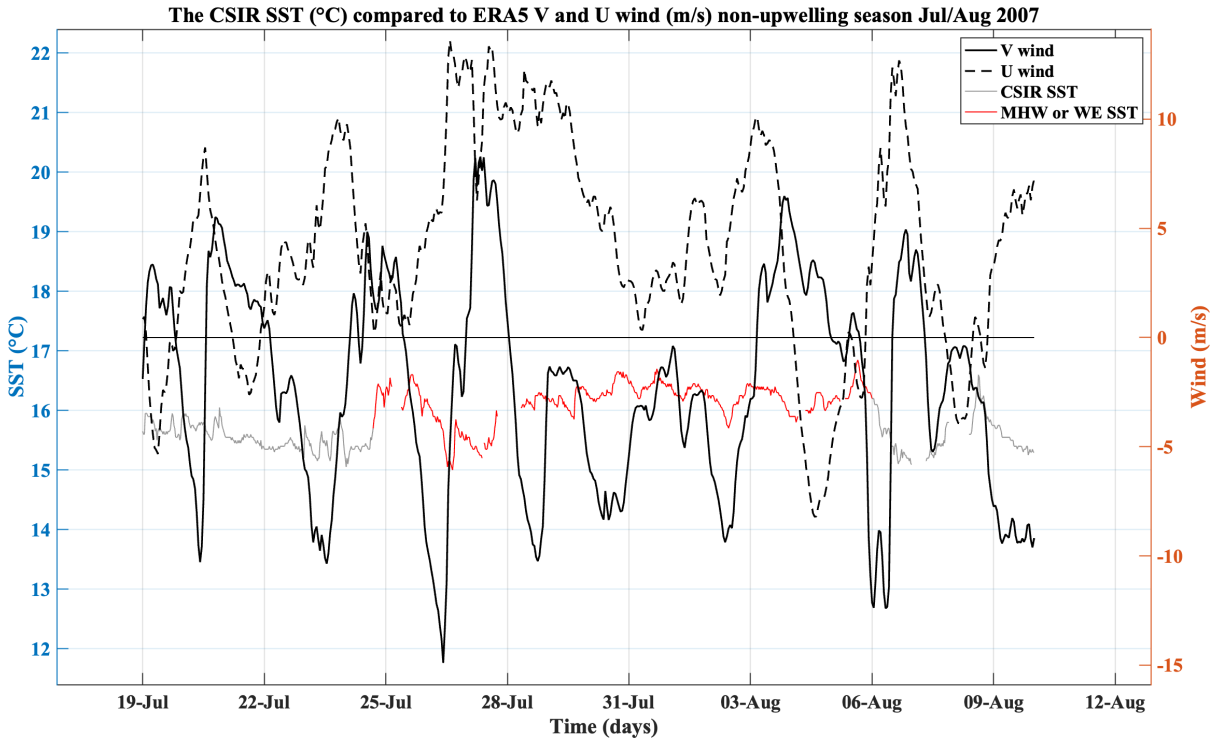

Figure 4. 17: CSIR SST (°C) and ERA5 wind (m s-1) are plotted in the non-upwelling season 2007 over Event 13 (24 July – 06 August, Table 2), at Cape Point CSIR station in the SBUS. Plotted is the original CSIR SST time series (grey), defined MHWs or WEs SST (red), V wind component (black) and U wind component (dashed black).

Figure 4.18 shows the spatial progression of the August 2007 MHW (Figure 4.17; Table 1 & 2) through CCI SST anomaly plots. On the day before the MHW and the day of the MHW, on the 23rd and 24th of July, at the CSIR mooring the SSTAs are between -1°C and 1°C with -3°C and -1°C SSTA values further offshore (Figure 4.18 A & B). On the 28th of July there are some SSTAs values between 1°C and 2°C slightly to the east of the CSIR mooring (Figure 4.18 C). On the 1st of August the SSTAs values between 1°C and 2°C have extended north-west over the CSIR mooring point (Figure 4.18 D). The day the CSIR MHW ends the area of the SSTAs values between 1°C and 2°C have decreased but still is over the CSIR mooring (Figure 4.18 E). The day after the CSIR MHW the SST around the CSIR mooring has decreased and the SSTAs are between -1°C and 1°C (Figure 4.18 F). In the REMSS dataset, there is a MHW to the north of the CSIR mooring which extends southwards during the August 2007 MHW moves northward towards the end of the MHW (Figure 8.5).

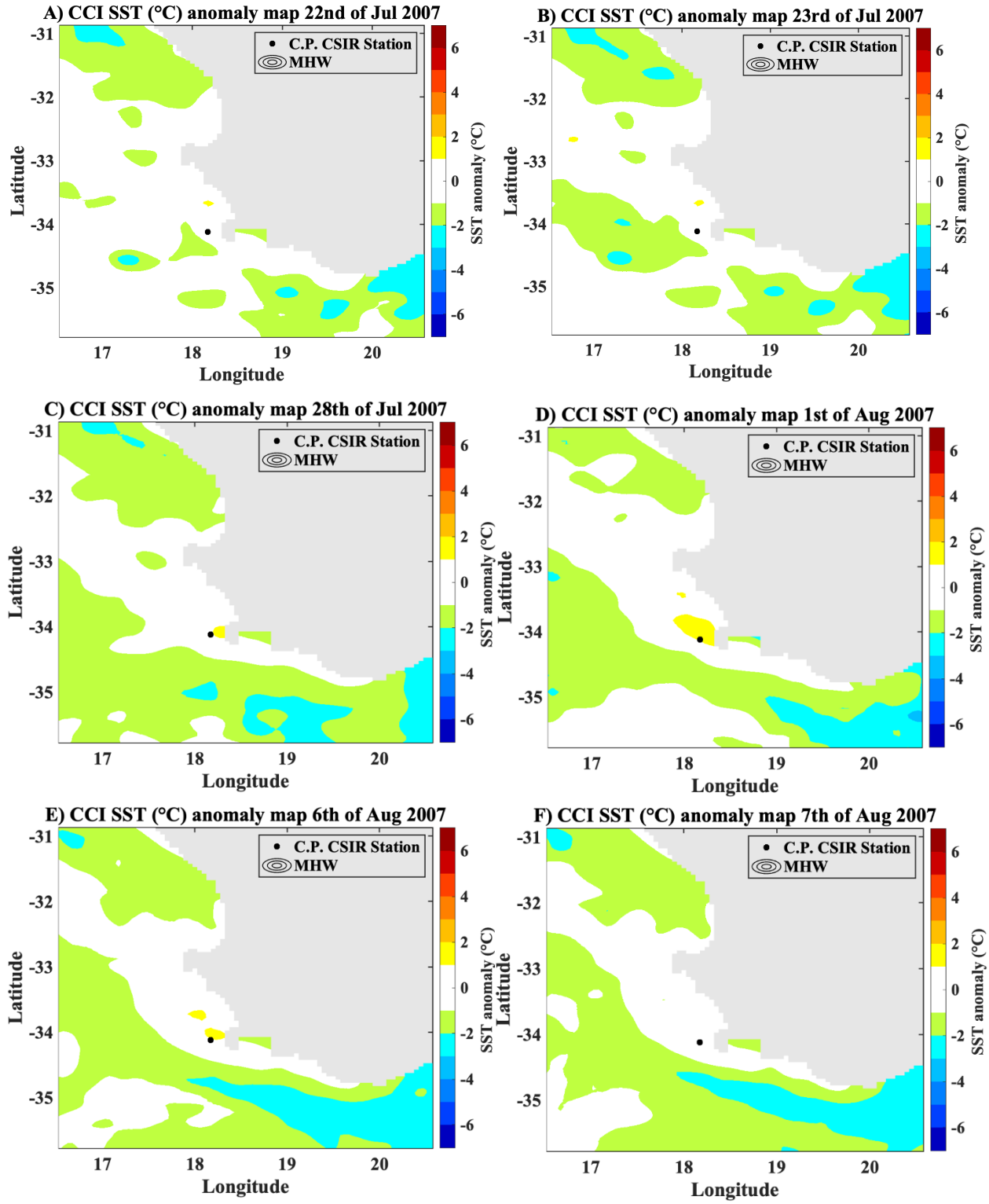

Figure 4. 18: July/August 2007 MHW event REMSS SST (°C) anomaly plots with MHW outline for A) the 23rd of July (1 day before MHW begins), B) the 24th of July (day MHW begins), C) the 28th of July (5 days after the start of the MHW), D) 1st of August (9 days after the start of the MHW), E) the 6th of August (day the MHW ends) and F) the 7th of August (1 day after MHW ends).

Chapter 5 – Discussion

In this chapter, first the characteristics of the climatological SST and MHWs at the CSIR mooring station will be discussed. Then the climatological states and MHW identification of satellite datasets, CCI and REMSS will be compared to *in situ* CSIR data. Lastly, the influence of the wind on the MHW formation and decay dynamics at the CSIR mooring will be compared between the upwelling and non-upwelling seasons.

5.1 MHWs at the CSIR mooring station

5. 1 A. The climatological state of SST at CSIR mooring station

It is widely accepted that the upwelling occurs most intensely in the summer, December, January and February, and also occurs in spring, September, October and November, in the Southern Benguela (Chavez & Messié, 2009; Tim et al., 2015). In the CSIR SST climatology the September monthly climatological average is closer to that of winter and the monthly climatological averages of March and April are even lower than the summer upwelling months. As the SST climatological averages are a product of not only upwelling but also the annual variation in solar radiation, March and April are not necessarily periods of increased upwelling but also the decrease in the higher SST values found in summer. As the interaction of upwelling and MHWs are still largely unknown in the Southern Benguela and the definition of a MHW is based on the climatological 90^{th} percentile, therefore the annual SST climatological cycle is separated into two six month seasons for the analysis of MHW events in this study. The upwelling season, from October to March, and the non-upwelling season, from April to September.

5.1 B. MHWs in the CSIR time series

At the CSIR mooring station from 2003 to March 2020, 14 MHWs were identified over the 17-years. One of the reasons for the total number of MHW events identified is the statistical definition of a MHW. The definition requires that the SST is above the 90^{th} percentile for at least five days. In the Southern Benguela the wind has cycles between 3 to 10 days as stated by Shannon and Nelson (1996). This means that either the events just fall short of the required number of days or goes below the 90^{th} percentile for a couple of hours and the event cannot be defined as a MHW. As Hobday et al. (2016) originally applied the definition to daily satellite time series, when using datasets with time scales smaller than a day it will change the number of MHWs identified. Hobday et al. (2016) also states that the definition is to be used as a

worldwide indicator, therefore if the number of days required for the definition of MHWs was less than five days then there are too many events identified in the tropics. This means that the statistical definition of a MHW may not be the most appropriate when applied to upwelling regions such as the Southern Benguela.

In order to understand extreme warm water events at the Cape Point CSIR mooring, this study will also be looking at WEs. The WEs are warm water events which have SST above the 90th percentile for at least 3 days. Three days was chosen not only because Hobday et al. (2016) considered using 3 days criteria for MHWs, but it also has been used in studies such as Meehl and Tebaldi (2004) to identify MHWs. The total number of events identified in the CSIR time series is 35 events, 21 of these events are WEs (Table 1). As seen in Figure 4.2 there are a few gaps in the CSIR *in situ* dataset, which could lead to the overlooking of some events at the CSIR mooring.

The number of events occurring in the upwelling season vs the non-upwelling season is different by one event, the upwelling season has 17 events and the non-upwelling season has 18 events (Figure 64.6 A & B). On average the MHWs and WEs in both the upwelling and non-upwelling seasons have a duration, the cumulative number of days per event, of 7 days (Figure 4.3). The event duration is less than the present predicted global model of MHW duration of 25 days, with a range of 15 to 33 days by Frölicher et al. (2018). Only two events fall into the global predicted duration, they are both MHWs occurring in non-upwelling 2007 (July and September; Figure 4.9 ; Table 1). In comparison to the upwelling season the non-upwelling season tends to have events which have a higher and a shorter duration. This would indicate in periods when upwelling is not occurring there is the potential for the MHWs to last longer in the Cape Peninsula Cell.

The MHW and WE events tend to last longer in the non-upwelling season but the events in the upwelling tend to have higher maximum temperatures. The mean maximum SST for the upwelling season is 20°C and for the non-upwelling season is 17.8°C. There is also a few degree difference in the highest maximum SST for each season, the highest maximum SST in the non-upwelling season is between 20°C to 21°C and is 23°C to 24°C in the upwelling. As austral summer is in the middle of the upwelling season, the solar radiation increase would be the most likely reason for the higher maximum temperatures. As an example of difference between the two seasons the two longest MHWs have a maximum SST of 16.6 °C and 16.55°C,

while the event with the high maximum temperature was a WE in the upwelling season in February 2012. Because extreme SSTs are dependent on the local climatology, anomalies are used to compare impact particularly on the marine environment. Therefore, the two longest MHWs have a SSTAs of 2.61°C and 2.6°C and the highest maximum SST WEs has a SSTA of 10.8°C (Table 1; Figure 1). Arafeh-Dalmau et al. (2019) and Frölicher and Laufkötter (2018) report that prolonged SSTAs > 6°C can cause irreversible ecosystem damages such as mass mortalities or regime shifts. This means that while MHWs or WEs occurring in the non-upwelling have the potential to last longer, the extremity of the MHWs SSTs is important to take into account.

5.2 A comparison of how SST products influence the MHW identification

The benefit of using the CSIR half-hourly time series is that processes which occur in time scales of a few hours are able to be captured, such as upwelling or MHW events. These events can be studied at a small time-scales with the CSIR mooring station data but we are not able to see how the events vary and/or progress spatially. The dataset is limited to the one mooring site. The benefit of satellite and reanalysis datasets is that variables, such as SST, are able to be studied over large regions. This means events such as MHWs can be understood in terms of spatial movement rather than at one mooring station. Unfortunately, satellite products do not capture variables, such as SST, well when close to the coast. This is stated by Lee and Park (2022) who have stated that the satellite OISST does well in the open ocean with less accuracy along the Korean coastal regions. As well as by Dufois et al. (2012) who state that pathfinder has a warm bias nearshore in EBUSs. As the Southern Benguela is a highly variable coastal system, understanding the impact of MHWs through satellite products will be challenging.

5.2 A) Satellite vs *in situ* products

The comparison of climatologies between the CSIR *in situ* data and CCI and REMSS satellite products can be seen in Figure 4.5. The product with the largest difference between *in situ* and satellite products is the REMSS time series, with the largest difference being about 6.5°C in February (Figure 4.5). Followed by the CCI dataset with a largest difference of 3°C in January (Figure 4.5). While the satellite products, particularly the CCI, do follow a more similar pattern during the non-upwelling season with SST values 1°C or 2°C higher than the *in situ* product. The satellite products show that the SST is higher in the upwelling season compared to the non-upwelling season, which is the opposite for the *in situ* CSIR product (Figure 4.5). This

would confirm that the CCI and REMSS satellite products are not able to capture the upwelling well close to the coast.

The over-estimation of the climatological SST will also affect the identification of MHWs as the definition of a MHW is dependent on the SST climatological state. The REMSS and CCI datasets have over double the number of events compared to the half-hourly CSIR with 70 and 88 MHW and WE events (Figure 4.6). In the upwelling season the REMSS time series has the most similar pattern of the number of MHW and WE identified per year to the half-hourly CSIR out of the satellite products (Figure 4.7). In the non-upwelling season the CCI product has the most similar pattern to half-hourly CSIR out of all the daily datasets (Figure 4.7). Although the satellite products were able to capture the MHW and WE half-hourly CSIR pattern, to varying degrees, this does not necessarily mean that the MHW and WE periods overlap with the half-hourly CSIR events. As an example, Figure 4.8 looks at the number of MHWs and WEs in 2003 as well as the period of the events. While a couple of events were at similar periods, the length and SST values differed and most of the events identified by the CCI and REMSS were not identified in the half-hourly CSIR. While satellite products can be useful when looking at SST over a large region, the CCI and REMSS datasets tend to overestimate the SST values, particularly during upwelling periods, and have an issue capturing upwelling and MHW and WE events.

5.2 B) Dataset timescales

While the satellite products identify over double the number of the MHWs and WEs, so does the CSIR daily time series. Converting the CSIR half-hourly dataset into a daily CSIR dataset doubles the number of MHWs and WEs detected from 35 events to 75 events (Figure 4.6). Therefore, the reason why the satellites do not have a similar number of events to the half-hourly CSIR may also be because of removal of daily variation in the daily products. As the SST product used in the sensitivity analysis by Hobday et al. (2016) is at a daily time scale, it also influenced the number of days which SST must be above the 90th percentile in order to classify as a MHW. The definition of a MHW will lead to varying results when applied to a sub-daily time scale rather than a daily time-scale. Therefore, when looking at MHWs at a sub-daily time scale a MHW definition which takes into account the daily variation will be required.

5.3 The influence of the wind on MHWs formation and dissipation

5.3 A) The Formation of MHWs and WEs

There are multiple potential drivers of MHWs as described by Gupta et al. (2020) such as intrusion of warm water. As the Agulhas current is in close proximity to the CSIR mooring it is more than probable that MHW events could be driven by the Agulhas leakage. This study looks at the influence of the wind on the formation and dissipation of the MHWs and WEs. In the CSIR time series 31 events (88.6%) of the 35 MHW and WE events identified in Table 2 begin with north-westerly winds (25 start with north-westerly winds and end with south-easterly winds). Of the 4 remaining events, 3 events begin with south-easterly winds, 2 of the events occur in the upwelling season and 1 event occurs with south-westerly winds in the non-upwelling season.

An example of a MHW onset driven by north-westerly winds is the September 2007 MHW (Figure 4.9), after the north-westerly wind blows for about a day the SST begins to warm and after a couple days the MHW begins. As seen in the CCI satellite anomaly plot there was warm water and a MHW just north-west of the CSIR mooring and the warm water moved over the mooring location (Figure). The September/October 2012 WE is similar to the September 2007 MHW as the onset is after a couple of days north-westerly winds with a MHW to the north of the mooring location (Figure 4.13 & 4.14). While the August 2003 WE does have a MHW near the mooring location the event also begins after a day of north-westerly and the CCI does show warm water above the mooring. While some of the events have north-westerly wind before the events, the SST tends to only respond when the north-westerly wind is above 7 m s^{-1}. This demonstrates a MHW or WE will only be formed with a north-westerly wind at the Cape Point mooring on the condition that there is warm water near the mooring which is transported to the region.

A MHW or WE starting with south-easterly winds is more likely to occur in the upwelling season, due to the dominance of south-easterly winds in summer as seen in the ERA5 wind climatology and as stated by Shannon and Nelson (1996). The March 2006 MHW is an example of an event which begins with south-easterly winds. The prolonged south-easterly winds above 6 m s^{-1} in the Southern Benguela should drive upwelling and the SST should be decreasing (Pagès et al., 1991). When looking at the CCI maps, a MHW moves towards the north-west into the South Atlantic and therefore this event could be caused by advection of

warm water rather than being wind driven. In order to confirm this further studies will be required.

The only event starting with south-westerly wind is the July/August 2007 event. While the onset of the event does begin with south-westerly winds there is north-westerly winds above 7 m s^{-1} just before the south-westerly winds. This means that the event could be caused by north-westerly winds with a delay in the response of the SST. However, it is also possible that the event was formed in a combination of north-westerly winds and low south-westerly winds. The south-westerly winds at the start of the event are around 3 m s^{-1} and therefore the reason for the MHW could also be surface warming. Surface warming MHWs are formed by low to no wind speeds, decreasing the turbulent heat fluxes from the ocean to the atmosphere (Holbrook et al., 2020). Which can lead to the build-up of heat from solar radiation in the ocean surface driving the SST to increase above the 90th percentile. Surface warming could also influence MHWs and WEs beyond the start of the event by increasing the duration and intensity of an event. This type of MHW formation is mostly likely to be to be found in the non-upwelling season where there is a tendency of lower wind speeds, as seen in the ERA5 climatology (Figure 4.1)

5.3 A. The Dissipation of MHWs and WEs

In EBUSs the frequency of coastal wind driven upwelling, by definition moves the surface waters offshore, should moderate the duration of MHWs or WEs in the coastal upwelling system (Varela et al., 2020). This theory seems to hold true for the Southern Benguela with 28 (80%) of 35 events ending with south-easterly winds, which are coastal upwelling driving winds (Hutchings et al., 2008). It is also important to note that only one event in the upwelling season did not end with south-easterly winds but north-westerly winds. In total there are 6 events which end with a north-westerly wind and 1 event which ends with a south-westerly wind.

In the example of the longest MHW, the September 2007 MHW, after 24 days of SST above the SST 90th percentile the SST decreases over 4°C in a day just after the south-easterly wind exceeds 9.8 m s^{-1}. The upwelling signal does not show in the CCI SST but there is a decrease in the SST but to climatologically average SST values. The March 2006 MHW, the possible advection event, is also ended by south-easterly wind and an upwelling event. While the CCI

March 2006 MHW remains persistent when the event ends in the CSIR time series, there are some upwelling signals further north along the coast. The events which are ended by upwelling are most likely to occur in the upwelling season seen in the ERA5 wind climatology that it is the period of south-easterly wind.

The events which are ended by south-westerly or north-westerly winds may have the same processes decreasing the SST. The September/October 2012 WE, ended during south-westerly winds and decreased just below the 90th percentile when the MHW ended and the SST remains around the same SST values for the following days. The August 2003 WE and the July/August 2007 MHW end with north-westerly winds and also end with the SST going just below the 90th percentile. The reason for the end of the events could either be that the warm SST is transported away from the mooring location or the SST is decreased by wind driven cooling. Strong winds increase the turbulent heat flux and vertical mixing which results in a decrease in the SST (Sen Gupta et al., 2020). For the August 2003 WE and the July/August 2007 MHW, the north-westerly wind exceeds 9 m s^{-1} and 12 m s^{-1} when the SST decreases. The CCI also shows a cooling of the SST surrounding the CSIR mooring. The September/October 2012 WE, ends during a 5.5 m s^{-1} south-westerly and the CCI plots show a decrease in the SST along the coast. The events which are ended by north-westerly or south-westerly winds are most likely to occur in the non-upwelling season seen in the ERA5 wind climatology that it is the period of north-westerly wind dominance.

5.3 C. MHW marine ecosystem impacts

How the MHWs and the WEs will affect the marine environment will depend on the response of the ecosystem to the occurrence, duration and maximum SSTs of the extreme warm water events. In the CSIR time series the number of events do not seem to be increasing over the 17-years from 2003 to 2020. It also seems that most of the events are within the 3 – 10 day wind cycle described by Shannon and Nelson (1996) with some exceptions in the non-upwelling season. While upwelling can be seen as moderator of the MHWs and WEs one of the rising concerns of MHWs is not only the long periods of high temperatures but also the fluctuation between MHW SSTs to lower SST values. Cabrerizo et al. (2021) states that fluctuations in SST can lead to changes in phytoplankton species. Van Der Walt et al. (2021) states that large changes can cause heart failure in fish species. This could be particularly harmful in the

Southern Benguela with cold water species in an environment where upwelling can cause SST values as low as 9°C and the highest SST value of the MHWs is 23°C.

It is also worth noting that the movement of warmer water masses into the Cape Peninsula Cell, depending on the timing, could increase productivity. Roy at al. (2001) studied a case study in the summer of 1999 to 2000, where the Southern Benguela had the highest anchovy recruitment recorded at least the last 15 years prior. In the middle of December (1999) there were strong, prolonged north/north-westerly winds observed, followed by strong and sustained south-easterly winds. The result of the atmospheric conditions was the transport of Agulhas water onto the west coast continental shelf. As the Anchovy eggs and larvae are transported by a coast jet into the west coast spawning grounds (in January-April), Roy at al. (2001) poses that the north-westerly winds "drastically reduced the advective loss of larvae". Additionally the intense upwelling (January-February 2000) following the high recruitment sustained a high level of primary and secondary production. This means that if a wind-driven extreme warm water event occurs during the transport of fish larvae from the Agulhas Current, followed by upwelling, there could be an increase in the marine biomass.

Chapter 6 – Conclusion

As MHWs are expected to increase in frequency, duration and maximum temperature, it is important to understand the characteristics of MHWs, how to identify and compare the events using different datasets and how they form and dissipate locally in the Cape Peninsula upwelling cell. The total number of MHWs, which exceed the SST 90th percentile for at least 5 days, in the 17-year CSIR SST time series is 14 events. As the Southern Benguela is a highly variable region, and this study is using half-hourly data rather than daily, WEs are also identified and defined as events which exceed the SST 90th percentile for at least 3 days. In total 35 MHWs and WEs were identified with no identifiable pattern indicating an increase in the occurrence of MHWs in both the upwelling vs non-upwelling season or the annual comparison. The MHWs and WEs have an average duration of 7 to 8 days, with the non-upwelling season having a tendency to have more events lasting shorter or longer than the upwelling season. The MHW SST values tend to be higher in the upwelling season, with the average maximum MHW temperature being 20°C while the non-upwelling season has an average below 18°C. This means that the MHWs which occur in the upwelling season will most likely be shorter than the non-upwelling season but will also tend to have higher SST values.

In order to understand how MHWs and WEs move spatially, using satellite products are effective however when close to the coast and in regions of high variability they are unable to efficiently capture SSTs. Proof of this concept can be seen in mean SST climatologies of REMSS and CCI which shows higher SST values in the summer than in the winter in the Cape Peninsula Upwelling Cell. The REMSS has the largest difference in the climatological means by 6.5°C, this difference in SST observations will continue into the 90th percentile climatologies and affect the identification of MHWs and WEs. REMSS and CCI both identify over double the amount of MHW and WE events than the CSIR half-hourly dataset. It is also worth noting that the events are being identified and compared over whole seasons and may not overlap in the same period. The inability of the satellite products to identify MHW and WE events at the same period as the half-hourly CSIR time series may not only be due to the issue with satellites capturing SST but also because of the different timescales of the datasets, even the daily CSIR has over double the number of half-hourly CSIR events. This highlights the

problem with using a daily definition for sub-daily timescales when identifying MHWs and WEs.

There are multiple potential drivers of MHWs as described by Gupta et al. (2020) such as the intrusion of warm water. As the Agulhas Current is in close proximity to the CSIR mooring it is more than probable that MHW events could be driven by the Agulhas leakage. This study looks at the influence of the wind on the formation and dissipation of the MHWs and WEs. The dominant wind, 88.6%, driving the formation of the MHWs and WEs is the north-westerly wind and a few events driven by south-easterly and south-westerly winds. The south-easterly wind is the dominant wind ending the MHW and WE events occurring during 80% of the events, the rest of the events occurred during north-westerly and south-westerly winds. It is important to note that while the wind may have some direct impact on the SST, such as wind driven cooling or surface warming, the changes in SST to form or dissipate the MHW or WE will most likely be from water masses either off the coast, surrounding surface areas or below the surface layer of the CSIR mooring location. Therefore, due to the dominance of the south-easterly wind regimes in the Cape Peninsula Cell, particularly in the upwelling-season, there is a natural limit to the duration of MHW and WEs. Going forward more research should be done on the drivers of MHWs and how the events differ throughout the Southern Benguela.

Chapter 7 – References

Abrahams, A., Schlegel, R. and Smit, A. 2021. Variation and Change of Upwelling Dynamics Detected in the World's Eastern Boundary Upwelling Systems. *Frontiers in Marine Science*. 8.

Adam, O., Bischoff, T. and Schneider, T. 2016. Seasonal and interannual variations of the energy flux equator and ITCZ. Part I: Zonally averaged ITCZ position. *Journal of Climate*. *29*(9): 3219-3230.

Ahmad, K.A., Jones, W.L., Kasparis, T., Vergara, S.W., Adams, I.S. and Park, J.D. 2005. Oceanic rain rate estimates from the QuikSCAT Radiometer: A Global Precipitation Mission pathfinder. *Journal of Geophysical Research: Atmospheres*. 110(D11).

Ali, M.M., Jagadeesh, P.S.V., Jain, S. 2007. Effects of eddies on bay of Bengal cyclone intensity. *Eos, Transactions, American Geophysical Union*. 88(8): 93-104.

Andrews, W.R.H. and Hutchings, L. 1980. Upwelling in the southern Benguela Current. *Progress in Oceanography*. *9*(1):1-81.

Arafeh-Dalmau, N., Montaño-Moctezuma, G., Martínez, J., Beas-Luna, R., Schoeman, D. and Torres-Moye, G. 2019. Extreme Marine Heatwaves Alter Kelp Forest Community Near Its Equatorward Distribution Limit. *Frontiers in Marine Science*. 6.

Barange, M. and Pillar, S.C. 1992. Cross-shelf circulation, zonation and maintenance mechanisms of Nyctiphanes capensis and Euphausia hanseni (Euphausiacea) in the northern Benguela upwelling system. *Continental Shelf Research*. *12*(9):1027-1042.

Bulgin, C.E., Embury, O. and Merchant, C.J. 2016. Sampling uncertainty in gridded sea surface temperature products and Advanced Very High Resolution Radiometer (AVHRR) Global Area Coverage (GAC) data. *Remote Sensing of Environment*. 177:287-294.

Cabrerizo, M.J., Marañón, E., Fernández-González, C., Alonso-Núñez, A., Larsson, H. and Aranguren-Gassis, M. 2021. Temperature fluctuation attenuates the effects of warming in estuarine microbial plankton communities. *Frontiers in Marine Science*. 8:656282.

Castelao, R.M. and Barth, J.A. 2006. Upwelling around Cabo Frio, Brazil: The importance of wind stress curl. *Geophysical Research Letters*. 33(3).

Chavez, F. and Messié, M. 2009. A comparison of Eastern Boundary Upwelling Ecosystems. Progress in Oceanography. 83(1-4):80-96.

Chu, P.C. 2015. Ekman spiral in a horizontally inhomogeneous ocean with varying eddy viscosity. *Pure and Applied Geophysics*. 172(10):2831-2857.

Ciani, D., Rio, M.H., Nardelli, B.B., Etienne, H. and Santoleri, R. 2020. Improving the altimeter-derived surface currents using sea surface temperature (SST) data: A sensitivity study to SST products. *Remote Sensing*. 12(10):1601.

Cochrane, K., Augustyn, C., Fairweather, T., Japp, D., Kilongo, K., Iitembu, J., Moroff, N., Roux, J., Shannon, L., Van Zyl, B. and Vaz Velho, F. 2009. Benguela Current Large Marine Ecosystem—Governance and Management for an Ecosystem Approach to Fisheries in the Region. *Coastal Management*. 37(3-4):235-254.

Confluence ECMWF. 2021. *ERA5: data documentation - Copernicus Knowledge Base - ECMWF Confluence Wiki*. [online] Available at: <https://confluence.ecmwf.int/display/CKB/ERA5%3A+data+documentation#ERA5:datadocumentation-Introduction> [Accessed 28 November 2021].

Copernicus. 2021. *Copernicus Climate Data Store | Copernicus Climate Data Store*. [online] Available at: <https://cds.climate.copernicus.eu/cdsapp#!/dataset/reanalysis-era5-pressure-levels?tab=overview> [Accessed 28 November 2021].

Council for Scientific and Industrial Research (CSIR). 2021. *Council for Scientific and Industrial Research (CSIR) - Overview*. [online] Available at: <https://nationalgovernment.co.za/units/view/212/council-for-scientific-and-industrial-research-csir> [Accessed 28 November 2021].

Dufois, F. and Rouault, M. 2012. Sea surface temperature in False Bay (South Africa): Towards a better understanding of its seasonal and inter-annual variability. *Continental Shelf Research*. 43:24-35.

Dufois, F., Penven, P., Whittle, C.P. and Veitch, J. 2012. On the warm nearshore bias in Pathfinder monthly SST products over Eastern Boundary Upwelling Systems. *Ocean Modelling*. 47:113-118.

ECMWF. 2021. *ERA5*. [online] Available at: <https://www.ecmwf.int/en/forecasts/datasets/reanalysis-datasets/era5> [Accessed 28 November 2021].

ECMWF. 2023. *ERA5*. [online] Available at: <https://confluence.ecmwf.int/pages/viewpage.action?pageId=133262398> [Accessed 2 January 2023].

Espinoza Morriberón, D. 2018. Interannual and decadal variability of the primary productivity and oxygen Minimum Zone in the Peruvian Upwelling System (Doctoral dissertation, Sorbonne université).

Frölicher, T. L., Fischer, E. M., and Gruber, N. 2018. Marine heatwaves under global warming. *Nature.* 560:360. DOI: 10.1038 s-141586-018-0383-9

Frölicher, T.L. and Laufkötter, C. 2018. Emerging risks from marine heat waves. *Nature communications*. *9*(1):1-4.

Garzoli, S.L. and Gordon, A.L. 1996. Origins and variability of the Benguela Current. *Journal of Geophysical Research: Oceans*. 101(C1):897-906.

GEBCO. 2021. *GEBCO Data Download*. Available: <https://download.gebco.net> [2021, September 27].

Goubanova, K., Illig, S., Machu, E., Garçon, V. and Dewitte, B. 2013. SST subseasonal variability in the central Benguela upwelling system as inferred from satellite observations (1999–2009). *Journal of Geophysical Research: Oceans*. 118(9): 4092-4110.

Grote, B., Ekau, W., Hagen, W., Huggett, J.A. and Verheye, H.M. 2007. Early life-history strategy of Cape hake in the Benguela upwelling region. *Fisheries Research*. 86(2-3), :179-187.

Hardman-Mountford, N.J., Richardson, A.J., Agenbag, J.J., Hagen, E., Nykjaer, L., Shillington, F.A. and Villacastin, C. 2003. Ocean climate of the South East Atlantic observed from satellite data and wind models. *Progress in Oceanography*. 59(2-3), :181-221.

Hobday, A.J., Alexander, L.V., Perkins, S.E., Smale, D.A., Straub, S.C., Oliver, E.C., Benthuysen, J.A., Burrows, M.T., Donat, M.G., Feng, M. and Holbrook, N.J. 2016. A hierarchical approach to defining marine heatwaves. *Progress in Oceanography*. 141:227-238.

Holbrook, N., Scannell, H., Sen Gupta, A., Benthuysen, J., Feng, M., Oliver, E., Alexander, L., Burrows, M., Donat, M., Hobday, A., Moore, P., Perkins-Kirkpatrick, S., Smale, D., Straub, S. and Wernberg, T. 2019. A global assessment of marine heatwaves and their drivers. *Nature Communications*. 10(1).

Hutchings, L., van der Lingen, C., Shannon, L., Crawford, R., Verheye, H., Bartholomae, C., van der Plas, A., Louw, D., Kreiner, A., Ostrowski, M., Fidel, Q., Barlow, R., Lamont, T., Coetzee, J., Shillington, F., Veitch, J., Currie, J. and Monteiro, P. 2009. The Benguela Current: An ecosystem of four components. *Progress in Oceanography*. 83(1-4):15-32.

Imbol Koungue, R., Rouault, M., Illig, S., Brandt, P. and Jouanno, J. 2019. Benguela Niños and Benguela Niñas in Forced Ocean Simulation From 1958 to 2015. *Journal of Geophysical Research: Oceans*. 124(8):5923-5951.

Kämpf, J. and Chapman, P. 2016. Upwelling Systems of the World. A Scientific Journey to the Most Productive Marine Ecosystems. *Springer International Publishing*.

Lee, E.Y. and Park, K.A. 2020. Validation of satellite sea surface temperatures and long-term trends in Korean coastal regions over past decades (1982–2018). *Remote Sensing*. 12(22):3742.

Lutjeharms, J.R.E. and Van Ballegooyen, R.C. 1988. The retroflection of the Agulhas Current. *Journal of Physical Oceanography*. 18(11):1570-1583.

Marbà, N., Jordà, G., Agustí, S., Girard, C. and Duarte, C.M., 2015. Footprints of climate change on Mediterranean Sea biota. *Frontiers in Marine Science*. *2*:56.

Meehl, G.A. and Tebaldi, C. 2004. More intense, more frequent, and longer lasting heat waves in the 21st century. *Science*. 305(5686):994-997.

Merchant, C.J., Embury, O., Roberts-Jones, J., Fiedler, E., Bulgin, C.E., Corlett, G.K., Good, S., McLaren, A., Rayner, N., Morak-Bozzo, S. and Donlon, C. 2014. Sea surface temperature datasets for climate applications from Phase 1 of the European Space Agency Climate Change Initiative (SST CCI). *Geoscience Data Journal*. 1(2):179-191.

Mohrholz, V., Bartholomae, C.H., Van der Plas, A.K. and Lass, H.U. 2008. The seasonal variability of the northern Benguela undercurrent and its relation to the oxygen budget on the shelf. *Continental Shelf Research*. 28(3):424-441.

NASA. 2023. *Ghrsst Level 4 MW_IR_OI Global Foundation Sea Surface Temperature Analysis Version 5.0 from REMSS| Physical Oceanography Distributed Active Archive Center (PO.DAAC). [online]*. Available at: <https://podaac.jpl.nasa.gov/dataset/MW_IR_OI-REMSS-L4-GLOB-v5.0 > [Accessed 20 January, 2023].

Oliver, E.C., Donat, M.G., Burrows, M.T., Moore, P.J., Smale, D.A., Alexander, L.V., Benthuysen, J.A., Feng, M., Sen Gupta, A., Hobday, A.J. and Holbrook, N.J., 2018. Longer and more frequent marine heatwaves over the past century. *Nature communications*. *9*(1):1-12.

Pagès, F., Verheye, H., Gili, J. and Flos, J. 1991. Short-term effects of coastal upwelling and wind reversals on epiplanktonic cnidarians in the southern Benguela ecosystem. *South African Journal of Marine Science*. 10(1):203-211.

Philippon, N., Rouault, M., Richard, Y. and Favre, A. 2012. The influence of ENSO on winter rainfall in South Africa. *International Journal of Climatology*. 32(15):2333-2347.

Reason, C.J.C. and Rouault, M. 2005. Links between the Antarctic Oscillation and winter rainfall over western South Africa. *Geophysical research letters*. 32(7).

Reynolds, R.W., Smith, T.M., Liu, C., Chelton, D.B., Casey, K.S., Schlax, M.G., 2007. Daily high-resolution-blended analyses for sea surface temperature. *Journal of Climate.* 20:5473–5496.

Risien, C., Reason, C., Shillington, F. and Chelton, D. 2004. Variability in satellite winds over the Benguela upwelling system during 1999-2000. *Journal of Geophysical Research: Oceans.* 109.

Rouault, M., Pohl, B. and Penven, P. 2010. Coastal oceanic climate change and variability from 1982 to 2009 around South Africa. *African Journal of Marine Science*. 32(2): 237-246.

Schlegel, R. and Smit, A. 2016. Climate Change in Coastal Waters: Time Series Properties Affecting Trend Estimation. *Journal of Climate*. 29(24):9113-9124.

Schlegel, R., Oliver, E., Hobday, A. and Smit, A. 2019. Detecting Marine Heatwaves With Sub-Optimal Data. *Frontiers in Marine Science*. 6.

Schlegel, R., Oliver, E., Perkins-Kirkpatrick, S., Kruger, A. and Smit, A. 2017. Predominant Atmospheric and Oceanic Patterns during Coastal Marine Heatwaves. *Frontiers in Marine Science*. 4.

Schlegel, R.W., Oliver, E.C., Wernberg, T. and Smit, A.J., 2017. Nearshore and offshore co-occurrence of marine heatwaves and cold-spells. *Progress in Oceanography*. 151:189-205.

Seabra, R., Varela, R., Santos, A.M., Gomez-Gesteira, M., Meneghesso, C., Wethey, D.S. and Lima, F.P. 2019. Reduced nearshore warming associated with eastern boundary upwelling systems. *Frontiers in Marine Science*. 6:104.

Selig, E.R., Casey, K.S., Bruno, J.F. 2010. New insights into global patterns of ocean temperature anomalies: implications for coral reef health and management. *Global Ecology and Biogeography.* 19:397–411.

Sen Gupta, A., Thomsen, M., Benthuysen, J., Hobday, A., Oliver, E., Alexander, L., Burrows, M., Donat, M., Feng, M., Holbrook, N., Perkins-Kirkpatrick, S., Moore, P., Rodrigues, R., Scannell, H., Taschetto, A., Ummenhofer, C., Wernberg, T. and Smale, D. 2020. Drivers and impacts of the most extreme marine heatwave events. *Scientific Reports*. 10(1).

Shannon, L. V. 1985. The Benguela ecosystem. I. Evolution of the Benguela, physical features and processes. *In Oceanography and Marine Biology*. 23:105-182.

Sorte, C.J.B., Fuller, A., Bracken, M.E.S. 2010. Impacts of a simulated heat wave on composition of a marine community. *Oikos.* 119:1909–1918.

Tim, N., Zorita, E., Schwarzkopf, F., Rühs, S., Emeis, K. and Biastoch, A. 2018. The Impact of Agulhas Leakage on the Central Water Masses in the Benguela Upwelling System From A High-Resolution Ocean Simulation. *Journal of Geophysical Research: Oceans*. 123(12):9416-9428.

Timmermann, A., An, S.I., Kug, J.S., Jin, F.F., Cai, W., Capotondi, A., Cobb, K.M., Lengaigne, M., McPhaden, M.J., Stuecker, M.F. and Stein, K. 2018. El Niño–southern oscillation complexity. *Nature*. 559(7715):535-545.

Tsamalis, C. and Saunders, R. 2018. Quality Assessment of Sea Surface Temperature from ATSRs of the Climate Change Initiative (Phase 1). *Remote Sensing*. 10(4):497.

Van Der Walt, K.A., Potts, W.M., Porri, F., Winkler, A.C., Duncan, M.I., Skeeles, M.R. and James, N.C. 2021. Marine Heatwaves Exceed Cardiac Thermal Limits of Adult Sparid Fish (Diplodus capensis, Smith 1884). *Frontiers in Marine Science*. 8:801.

Varela, R., Rodríguez-Díaz, L., de Castro, M. and Gómez-Gesteira, M. 2021. Influence of Eastern Upwelling systems on marine heatwaves occurrence. *Global and Planetary Change*. 196.

Veitch J., Penven Pierrick, Shillington F. 2010. Modeling equilibrium dynamics of the Benguela current system. *Journal of Physical Oceanography*. 40(9):1942-1964.

Waliser, D.E. and Gautier, C. 1993. A satellite-derived climatology of the ITCZ. *Journal of climate*. 6(11):2162-2174.

Wang, Y., Castelao, R.M. and Yuan, Y. 2015. Seasonal variability of alongshore winds and sea surface temperature fronts in Eastern Boundary Current Systems. *Journal of Geophysical Research: Oceans*. 120(3):2385-2400.

Wavenet. 2021. *WaveNet: The online real time wave and weather for South Africa: History*. [online] Available at: <http://wavenet.csir.co.za/history.htm> [Accessed 28 November 2021].

Weeks, S.J., Barlow, R., Roy, C. and Shillington, F.A. 2006. Remotely sensed variability of temperature and chlorophyll in the southern Benguela: upwelling frequency and phytoplankton response. *African Journal of Marine Science*. 28(3-4):493-509.

Chapter 8 – Appendix

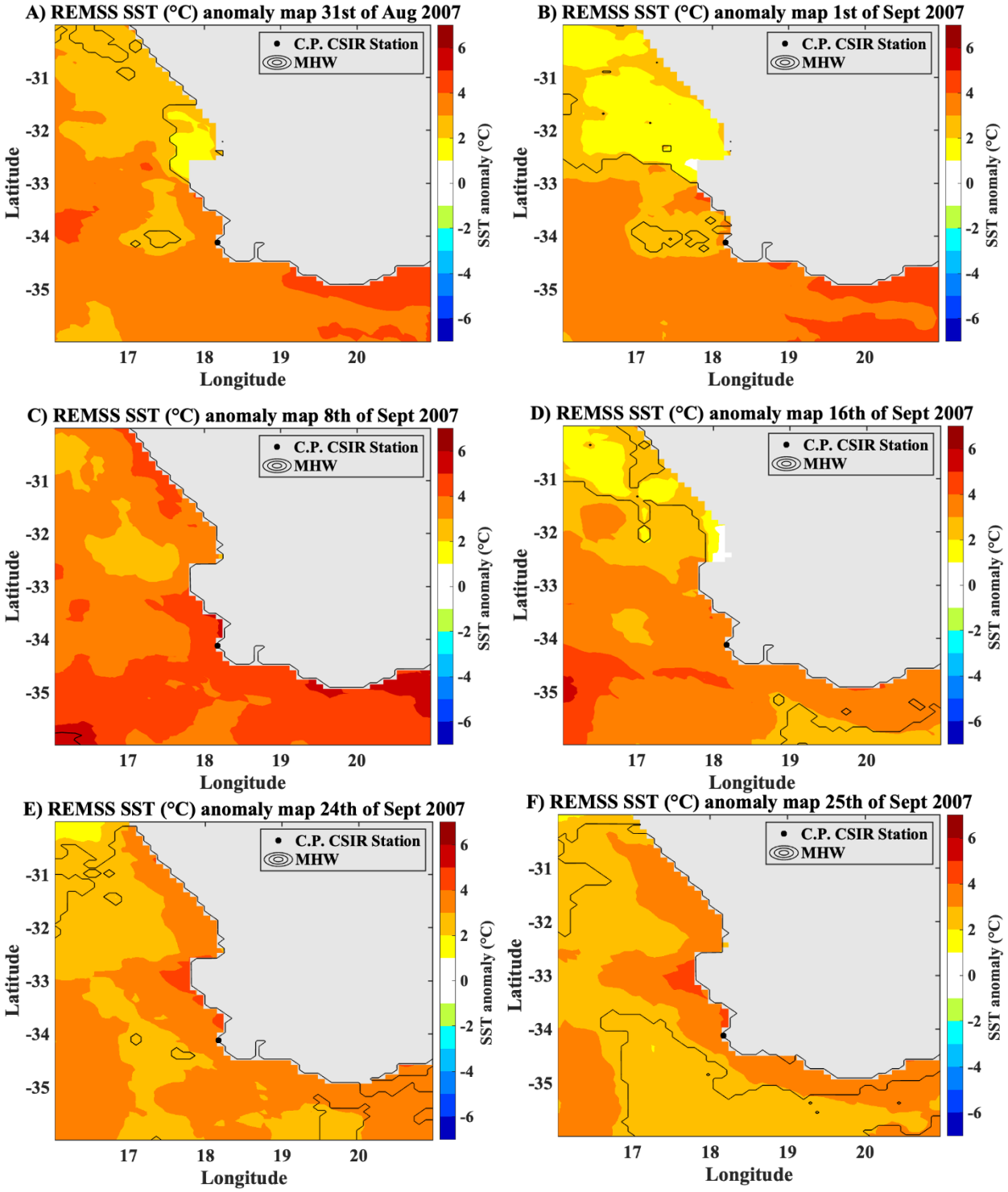

Figure 8.1: September 2007 MHW event REMSS SST (°C) anomaly plots with MHW outline for A) the 31st of August (1 day before MHW begins), B) the 1st of September (day MHW begins), C) the 8th of September (7 days after the start of the MHW), D) 16th of September (15 days after the start of the MHW), E) the 24th of September (day the MHW ends) and F) the 25th of September (1 day after MHW ends).

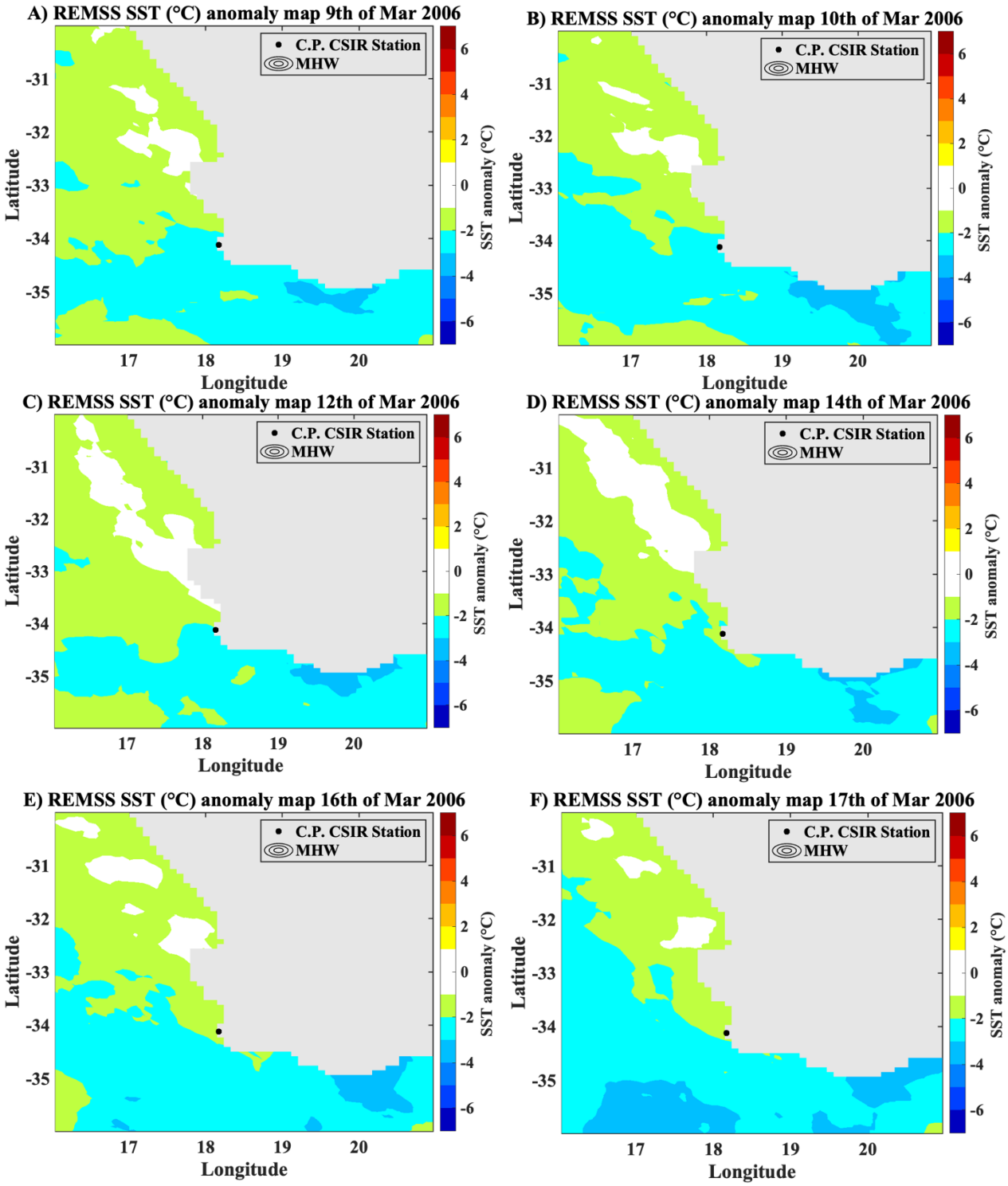

Figure 8.2: March 2006 MHW event REMSS SST (°C) anomaly plots with MHW outline for A) the 9th of March (1 day before MHW begins), B) the 10th of March (day MHW begins), C) the 12th of March (2 days after the start of the MHW), D) 14th of March (4 days after the start of the MHW), E) the 16th of March (day the MHW ends) and F) the 17th of March (1 day after MHW ends).

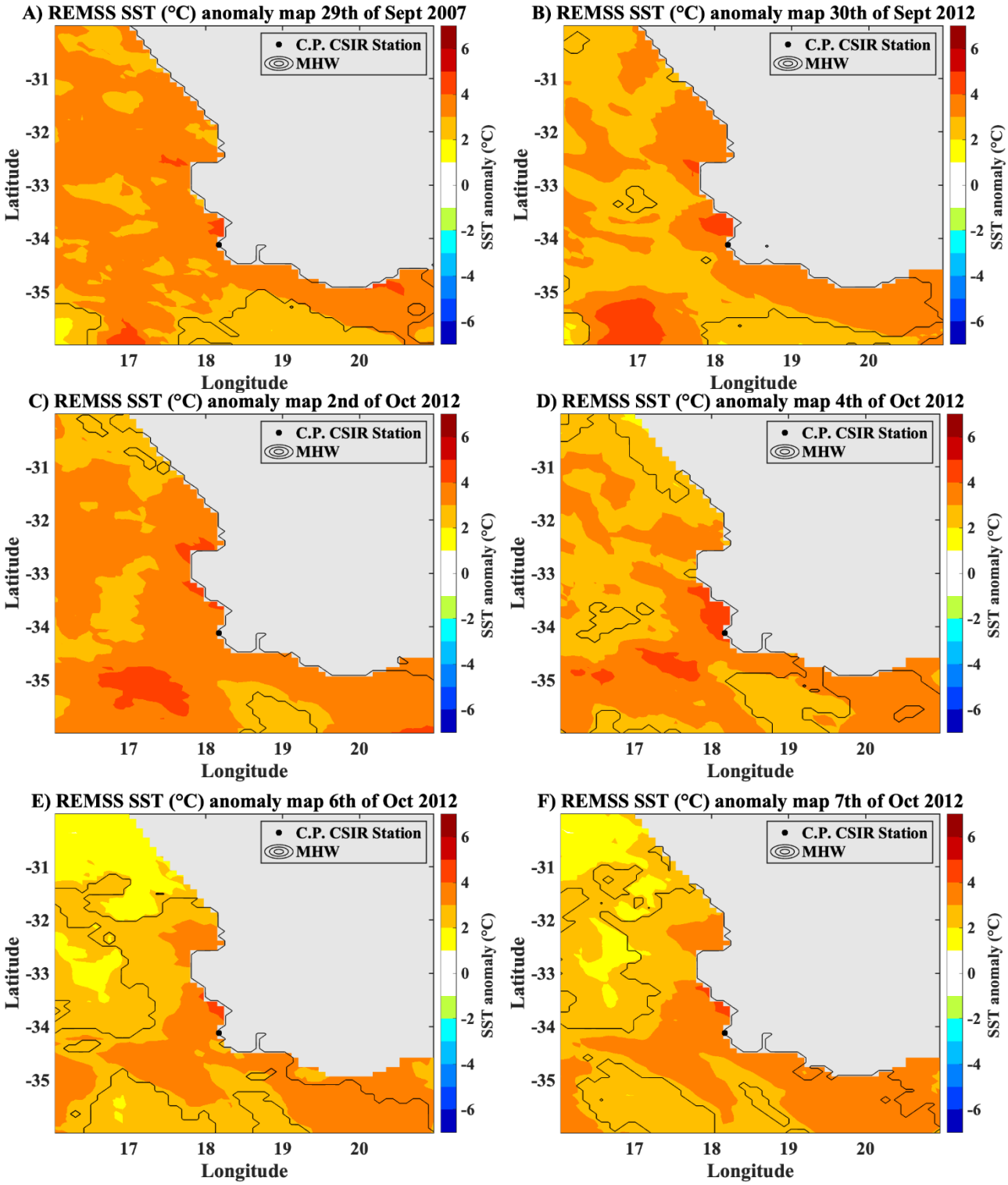

Figure 8.3: September/October 2012 WE event REMSS SST (°C) anomaly plots with WE outline for A) the 29th of September (1 day before WE begins), B) the 30th of September (day WE begins), C) the 2nd of October (2 days after the start of the WE), D) 4th of October (4 days after the start of the WE), E) the 6th of October (day the WE ends) and F) the 7th of October (1 day after WE ends).

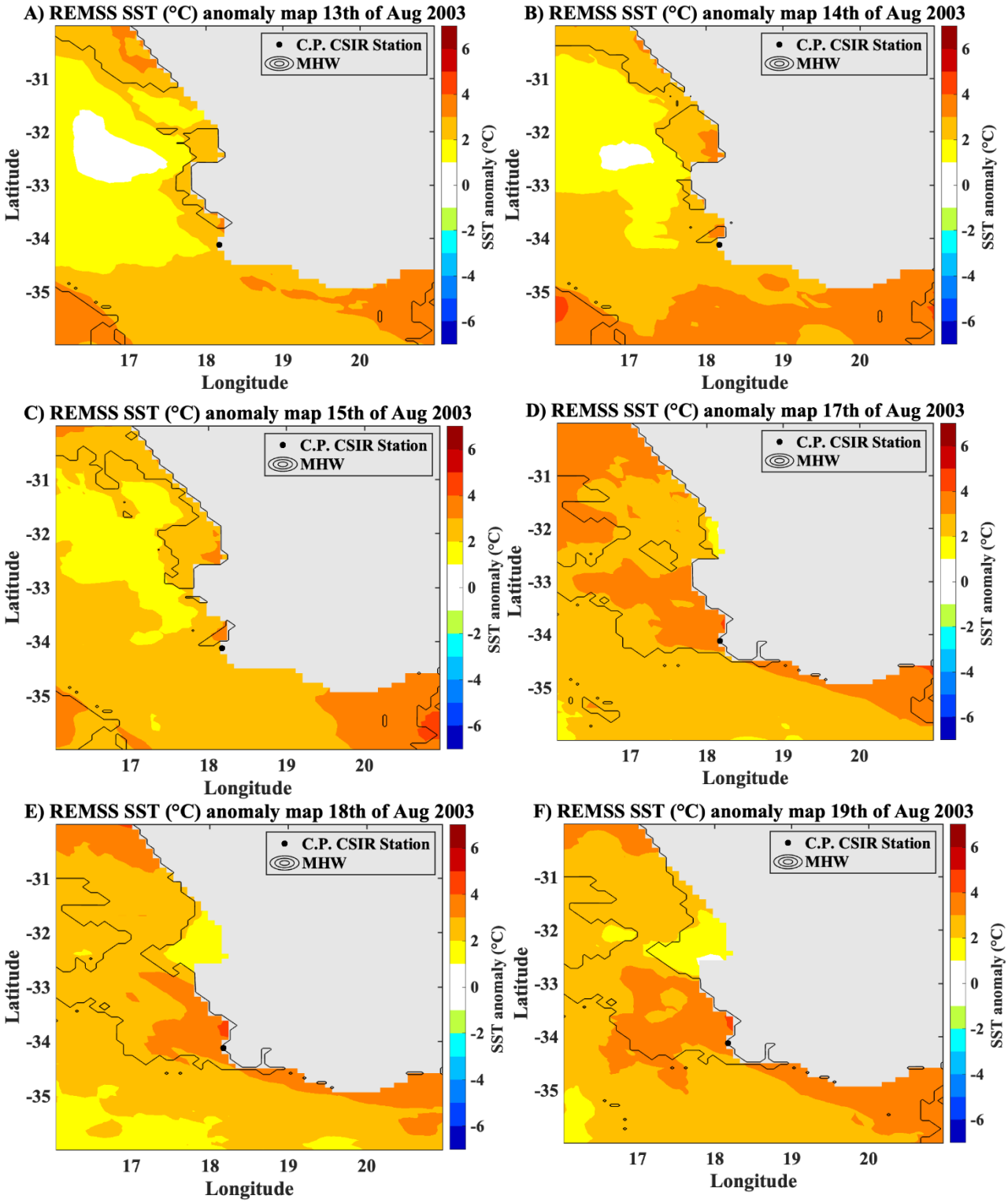

Figure 8.4: August 2003 WE event REMSS SST (°C) anomaly plots with WE outline for A) the 13th of August (1 day before WE begins), B) the 14th of August (day WE begins), C) the 15th of August (1 day after the start of the WE), D) 17th of August (3 days after the start of the WE), E) the 18th of August (day the WE ends) and F) the 19th of August (1 day after WE ends).

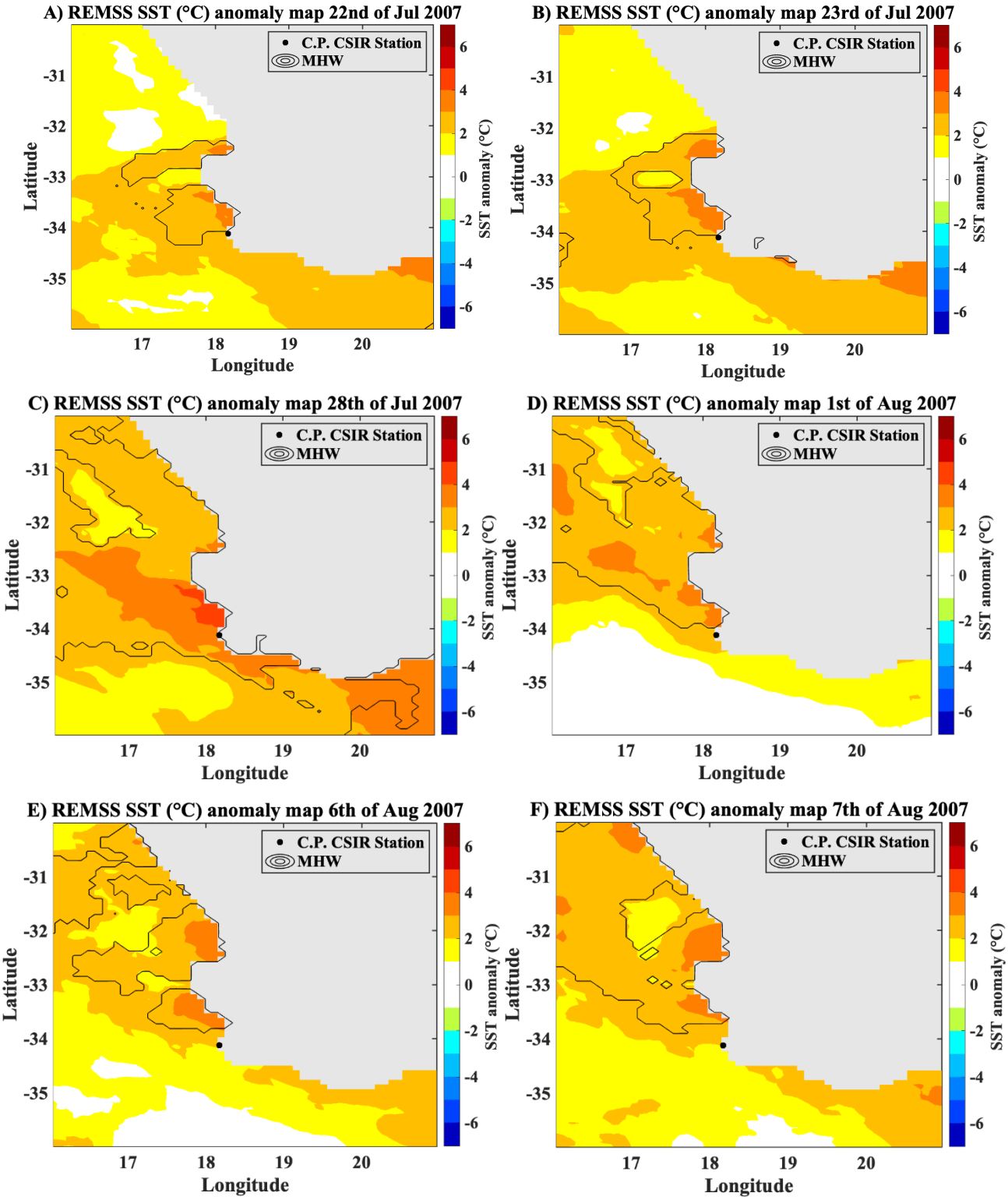

Figure 8.5: July/August 2007 MHW event REMSS SST (°C) anomaly plots with MHW outline for A) the 23rd of July (1 day before MHW begins), B) the 24th of July (day MHW begins), C) the 28th of July (5 days after the start of the MHW), D) 1st of August (9 days after the start of the MHW), E) the 6th of August (day the MHW ends) and F) the 7th of August (1 day after MHW ends).